# Tactor Factor
## A Pneumatic Tactile Display

# ME 450 Final Report

**Professor Brent Gillespie**
**April 21, 2009**

**Team 12**
**Louis Kratchman**
**Marc Michener**
**Timothy Minardi**
**Jian Wen**

# TABLE OF CONTENTS

## EXECUTIVE SUMMARY

Tactile displays convey information by mechanical stimulation of the skin and are an active research area with potential commercial applications in portable communication devices and haptic feedback devices. Previous approaches have achieved dense spacing of mechanical skin stimulators, but were often bulky and deficient in overall information transmission capability. Effective tactile displays must be matched to the perceptual limitations of the human tactile system, and scientific data on the skin's tactile response is incomplete. Our objective is to develop a tactile display exceeding the information bandwidth achieved by previous devices, which will allow further experimentation with actuator size and spacing while remaining portable and energy efficient.

We reviewed research on tactile perception and studied the limitations of available manufacturing processes to derive the following set of engineering specifications: output force greater than 500 mN, frequency of at least 50 Hz, skin displacement of at least 0.1 mm, 16 actuators, actuator diameter of 2 mm, 5 mm center-to-center actuator spacing, and a tactile pad thickness of 1-3 cm. The force, frequency, and indentation specifications are derived from research on the perceptual thresholds for vertical indentations of the fingertip. A frequency range of 18-56 Hz is considered ideal for tactile perception of spatially distributed stimuli on the fingertip [1], where force and indentation thresholds are at a minimum of 500 mN and 1mm [2] [3].

After performing an extensive review of tactile displays, we found only a few designs utilizing pneumatic actuation. Noting the potential for miniaturization of pneumatic components, we became interested in the potential of pneumatic displays for portable devices with high actuator density. After generating several concepts for pneumatic tactile displays employing lateral stimulation, we redirected our efforts towards development of a simpler pneumatic bubble display using stimulation in the vertical direction.

Our pneumatic bubble tactile display prototype features 16 independently-controllable bubbles, ranging from 1.2 mm to 1.8 mm in diameter. The bubbles were molded from polydimethylsiloxane (PDMS), a biocompatible polymer with favorable conformability to small mold parts. The bubbles were inflated with $CO_2$ gas at 0-30 psi, which was routed through 16 electro-pneumatic valves that oscillated the flow within the specified frequency specifications. The valves were controlled by a circuit consisting of a microcontroller with a bank of amplifying transistors, along with an array of LEDs for a parallel visual presentation of the tactile display.

In developing our display, we analyzed each of the subcomponents with appropriate models. We combined a model for the nonlinear displacement of pressurized bubbles with experimental data obtained by other researchers on the fingertip's mechanical impedance to predict the displacement of the skin as a function of bubble diameter, gas pressure, membrane thickness and other parameters. We also analyzed the fluid mechanics of the system, and used the results to guide selection of pneumatic components as well as design of the pad itself.

We tested our analytical models by measuring the bubble tip displacement of the completed device and compared it to our models which indicated a 30 percent greater experimental displacement. We also conducted a psychophysical experiment with human subjects, and found that smaller diameter bubbles (1.2 mm) were easiest to identify as separate stimuli. We also found that subjects had difficulty identifying the number of simultaneously inflated bubbles as the number increased.

We concluded that our control circuitry and use of electro-pneumatic valves were effective at regulating the gas flow, and that molded PDMS is a promising material for pneumatic bubble displays. With further experimentation on bubble size and spacing it should be possible to identify optimal bubble diameter and spacing, improving the display's capability to transmit information.

## ABSTRACT

Tactile displays convey information by mechanical stimulation of the skin and are an active research area with potential commercial applications in portable communication devices and haptic feedback devices. Current tactile display technologies are bulky, have high energy losses, and do not achieve optimal haptic stimulation. Our goal is to create a computer-controlled tactile display that transmits the maximum amount of information to the mind through the sense of touch. Our device will merge efficient energy conversion techniques with small-scale actuators to stimulate fingertip skin, and will provide a testing platform for further refinement of the technologies introduced. Also, we aim to reduce the size of the device in anticipation of future applications in portable devices.

## DESIGN SPECIFICATIONS

Our design specifications (Table 1) were derived from research on tactile perception as well as the limitations of available manufacturing methods. Force, displacement, frequency, spacing, and size specifications are based partly on thresholds for tactile perception under vertical displacements, further discussed in the tactile perception section below. The tactor size and spacing specifications are also based on our knowledge of the lower bounds of accurate machining with the manufacturing tools available to us. The thickness of the tactile pad was based on the intended use of the device as a portable and unobtrusive consumer device.

| Parameter | Specification |
|---|---|
| Output Force | 500 mN |
| Displacement | 0.1 mm |
| Frequency | 50 Hz |
| Tactor spacing | 1-5 mm |
| Tactor Size | 1-3 mm |
| Pad Thickness | 1-3 cm |

**Table 1:** Design specification for tactile array

## CUSTOMER REQUIREMENTS

Our project is not intended for immediate use in the consumer market, but is approached as a research tool towards future technological development. We therefore focused on only a few key customer requirements, leaving aside the finer details necessary for making the device ready for the marketplace:

- The stimuli should be perceivable.
- The device should be comfortable.
- The device should be safe for all users.
- The device should be durable and able to operate in a typical consumer environment.

The requirement that the device stimuli should be perceivable is most important because if the device is not perceivable, then the functionality of the device is lost. Since information takes time to convey, the comfort of the user while using the device must also be considered. Since the device is intended for eventual consumer use, safety and durability are also essential. These requirements formed the cornerstone of our design activity.

## REVIEW OF RELEVANT TOPICS

In order to create a competitive pneumatic tactile array, we reviewed tactile perception, other pneumatic arrays, pneumatic logic, and possible array materials. An expanded survey of additional non-pneumatic tactile array devices is presented in Appendix D.

### Tactile Perception

Tactile displays convey information through the sense of touch, so a review of prior research on tactile perception is essential to understanding the interaction of mechanical devices with the skin. Perception of skin displacements involves several types of nerve fibers and sensory structures, so the subjective response to mechanical stimulation is quite complex, depending on the location, magnitude, and frequency of stimulation as well as the size and shape of the object indenting the skin.

**Mechanoreceptors and perceptual thresholds:** As shown in Figure 1, Mechanoreceptors are sensory receptors under the skin that respond to mechanical displacement or distortion of the skin. There are four main types but we will be focusing into the two that are believed to have the greatest density and spatial resolution ability in the fingertip - Meissner corpuscles and Merkel Discs.

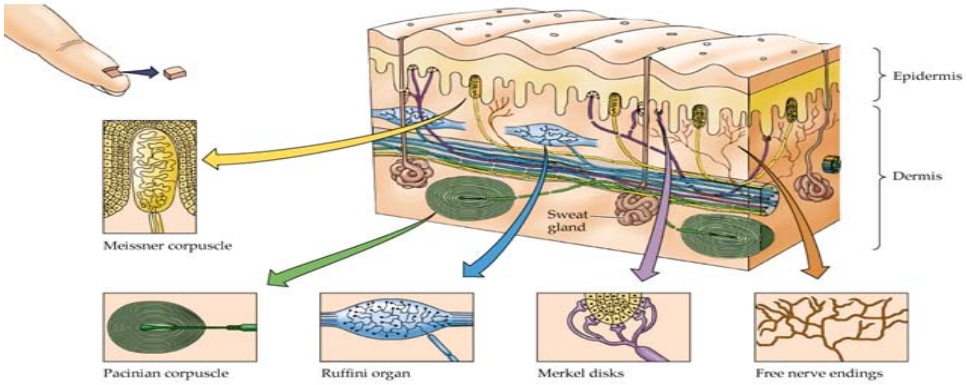


**Figure 1**: Afferent nerve fibers terminate in mechanoreceptors, tiny subcutaneous structures which have evolved to respond optimally to specific stimuli ranges [4].

Merkel discs respond primarily to pressure (either constant or changing with time) and are most sensitive to oscillatory disturbances at 1-3 Hz. Meissner corpuscles respond to skin displacement velocity and are most sensitive at 18 to 56 Hz [1]. The skin's frequency-dependent perceptual thresholds to normal displacements is summarized Fig. 2, where research on the individual responses of mechanoreceptors is combined into a single model [5].

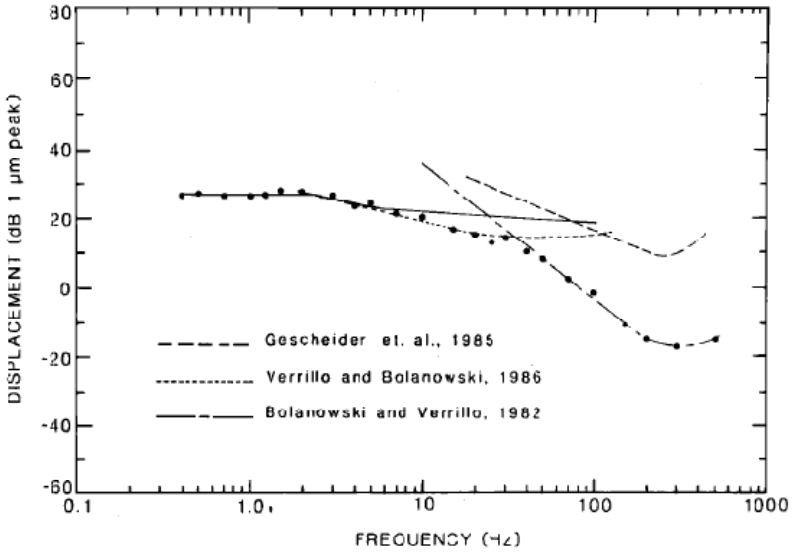


**Figure 2**: Skin indentation thresholds as function of frequency [5]. The large black dots represent the minimum perceptual threshold for displacement, while the various dotted lines represent the individual thresholds for the four mechanoreceptors found in the fingertip

**Two-point discrimination tests:** The minimum distance between two adjacent stimuli necessary to identify them as separate is a common benchmark in psychophysical experiments. The two-point discrimination test (TPDT) is a function of the indenting object's shape, displacement, applied force, and frequency, and is helpful in quantifying the spatial resolution possible under a given stimuli. Figure 3 shows experimental results which verify that spatial stimuli resolution is greatest when driving frequencies target the closely packed Meissner corpuscle and Merkel disc receptors, and shows that increasing the spacing between stimuli makes the discrimination task easier.

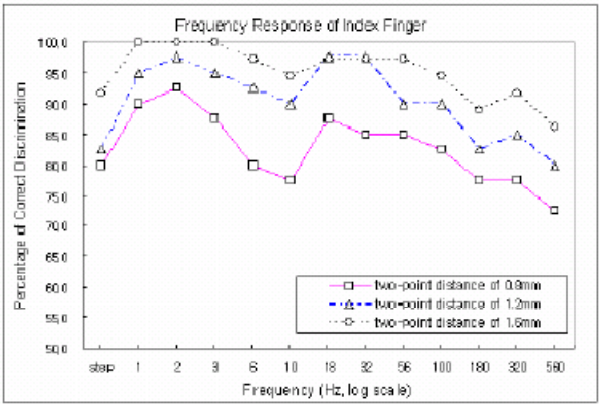


**Figure 3**: Two-point discrimination tests (TPDT's) for the fingertip under oscillatory stimulation [1]. Higher success rates are found in frequency bands corresponding to the peak responses of Meissner corpuscles and Merkel discs.

As tactile perception is clearly assisted by oscillatory stimulation, the implications for design of tactile displays are clear: spatial resolution can be maximized by tuning the driving frequency to the sensitivities of the mechanoreceptors responsible for fine tactile discrimination. Less is known, however, about the effects of the diameter and shape of the indenter on perceptual thresholds.

**Pneumatic Tactile Displays**

Pneumatic tactile displays use air pressure to displace the skin, either by inflating conformable tactors or discharging air directly through nozzles against the skin. Prior approaches to pneumatic displays separated the compressed air source and electronically-controlled valves from the tactile pad by lengths of flexible tubing. King et al. [6] recently developed a display to convey textural haptic feedback to users of a master-slave surgical robot, via an array of polydimethylsiloxane silicone (PDMS) bubbles at pressures up to 15 psi (Figure 2). Table 2 shows the authors' conclusions on optimal dimensions derived from psychophysical experiments. Subjects were able to discriminate between various combinations of two tactors with accuracies above 95 percent. A previous pneumatic approach by Kim et al. [7] tested an array of open nozzles to discharge compressed air directly against the skin (Figure 3). An external compressor provided constant pressure of 1.034 bar, gated through binary on/off computer-controlled valves. Psychophysical experiments showed error rates around 50 percent in distinguishing the locations of tactors. Another design involved using pneumatics to actuate pins that deflected through an elastic membrane and pressed on the skin as seen in Figure 4. The array had a max frequency of 5 Hz and could produce static displacements up to 0.7 mm [8].

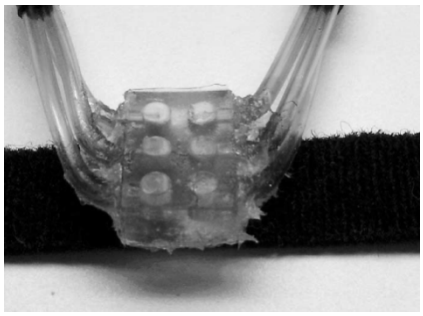

Figure 2: Pneumatic Bubble Array [6]

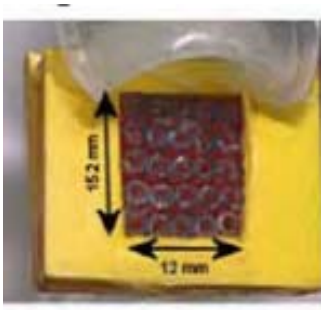


Figure 3: Air Jet Array [7]

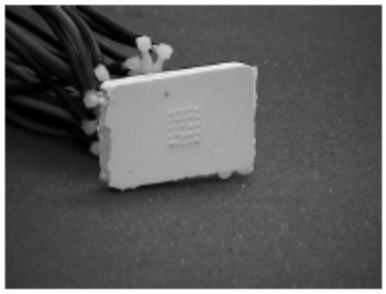

Figure 4: Pneumatic Pin Array [8]

| Tactile Display | Tactor Diameter | Tactor Spacing | Bandwidth | Tactor Array | Pad Thickness | Displacement or Force |
|---|---|---|---|---|---|---|
| Pneumatic Bubbles [6] | 3.0 mm | 1.5 mm (E) | 8-10 Hz | 3 x 2 | 0.4 cm | n/a |
| Air Jets [7] | 1.5 mm | 2.4- 3.2mm (C) | 0-50 Hz | 5 x 5 | n/a | n/a |
| Pneumatic Pins [8] | 1.02 mm | 2.5 mm | 0-5 Hz | 5 x 5 | n/a | 0.7 mm |

**Table 2:** Specifications of similar pneumatic tactile displays

Pneumatic energy delivery enables forces and displacements that readily exceed perceptual thresholds. However, the generally bulky equipment needed to generate, store, and gate compressed air presents portability challenges. Also, slow valve switching speeds and the latency inherent with transmitting signals through compressible gases limit the frequency ranges achieved thus far.

Wide-diameter tactors have generally been necessary in pneumatic tactile arrays to achieve perceptibility, due to the relatively flat pressure distributions produced. Tactors designed to produce more focused pressure may enable denser arrays. A recent pneumatic tactor design [9] introduced a corrugated elastomeric structure which deforms into a narrower shape than the membranes used to create bubbles in previous approaches.

## CONCEPT GENERATION

We began our concept generation with a functional decomposition of the tactile display concept into subcomponent systems. Figure 5 illustrates this analysis, which began with deriving concepts for lateral movement at the skin interface and later steered into the direction of producing normal indentation.

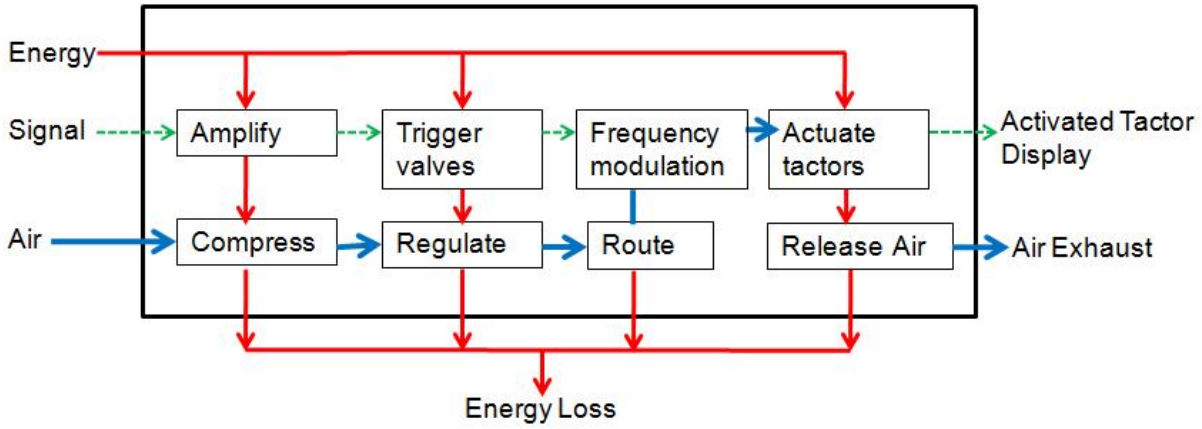


**Figure 5**: A pneumatic tactile display involves many potential energy losses

Our final working design will consist of an air supply, regulator, valves, tubing, and a tactile display. In order to produce a functional project, we will focus more on innovative design of the tactile array and use a basic setup for the air supply and valves. This main concentration on the array will allow for better and more complicated array designs, which can later be coupled with improved upstream designs (tank, regulator, and valves).

### Upstream of the Display

To simplify the design of the upstream components, many of our ideas involved an assembly of a compressed air tank, regulator, solenoid valves, manifolds, tubing, and connectors that will combine together as seen in Figure 6 below. Some designs even included pressure actuated valves to create relay logic and minimized the number of solenoid valves. This however took away the ability to actuate all tactors at one time and the design was dismissed. Other concepts involved the fabrication of piezoelectric actuated valves, but that would be a project in itself and were also dismissed. Each upstream component is available from manufacturers to eliminate extra design and fabrication. We will concentrate on minimizing component size when possible to increase the mobility of our array.

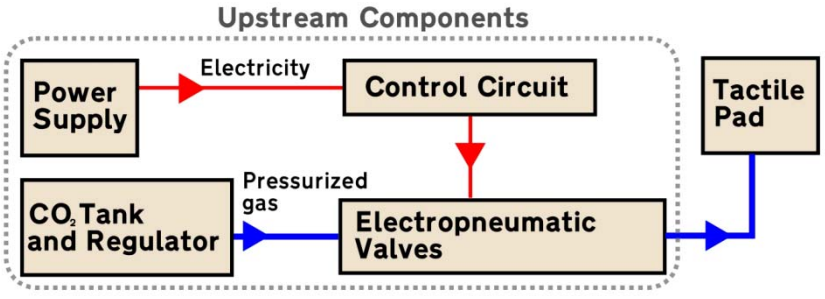


**Figure 6:** Block diagram showing role of upstream components

**Concept Generation for Pneumatic Tactile Displays**

To generate concepts for the tactors themselves, we considered both our spacing specifications and the limitations imposed by available manufacturing techniques. At the required size, most traditional material shaping techniques are impractical. Instead we considered the use of computer-controlled devices, such as the laser cutter and CNC mill, as well as microfabrication techniques used to create microelectromechanical systems (MEMS). For most processes available to us, material removal and deposition is conducted in the plane.

Many of our designs utilized the pneumatic bubble, a simple air pressure-to-mechanical energy transducer which can be linked with other mechanism, and simply manufactured by adhering a membrane layer over holes. An expanded discussion of concepts entertained is presented in Appendix C.

Our first concept involved horizontal pneumatic pistons, and alerted us to the restrictions of small-scale fabrication. We envisioned a plane with horizontal cylindrical holes bored into it, with notches exposing the surface of the plane. As shown in Fig. 7 Tiny pistons designed with vertical protrusions to stretch the skin laterally would be powered by jets of air. While this design would provide pure lateral motion with a large travel distance, the complexities of manufacturing such a device with adequate precision seemed daunting to us. In addition to fitting the pistons to the holes, we would need tiny sliding flaps covering the exposed notch in the holes to prevent air leakage.

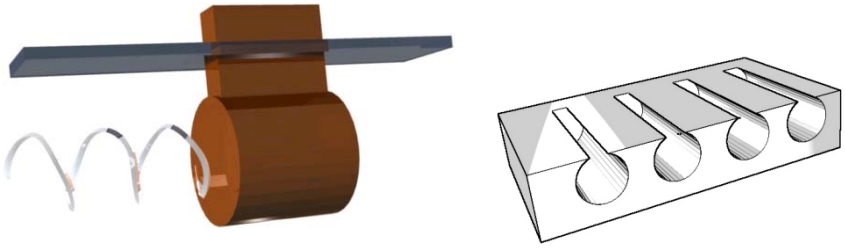

**Figure 7**: A piston with covering (left) travels horizontally in cylindrical holes (right)

Recognizing the simplicity of the bubble concept, but dismayed by the difficulty of converting its vertical motion to lateral, we next proposed manufacturing bubbles in a plane, and then slicing the plane into strips to create rows of horizontal bubbles. A segment of a row is shown in Fig. 8, where the horizontal motion would be amplified through a lever to enhance perceptability. The lever shown represents the general geometry of our intended mechanism, elaborated in further iterations mentioned in the appendix. While dividing a plane of bubbles into strips is possible, realigning and securely attaching it to underlying tubing would be a severe challenge.

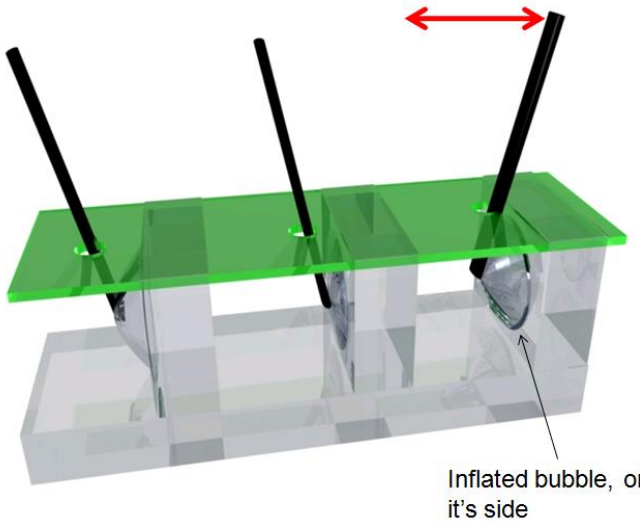


**Figure 8**: Bubbles deflect in the horizontal direction to ease production of lateral motion

As an alternative to the simple round bubble, we considered alternative shapes for inflation chambers that could produce lateral motion, shown in Figure 9. Inspired by the Bourdon Tube mechanism used in mechanical pressure gauges, we designed a crescent-shaped chamber which would reside in a plane. When inflated, it would stretch out, while a vertically protruding pick would grip and stretch the skin. While such devices would efficiently produce lateral motion, molding the chambers at the scales required and attaching them to a manifold horizontally was deemed beyond our fabrication abilities.

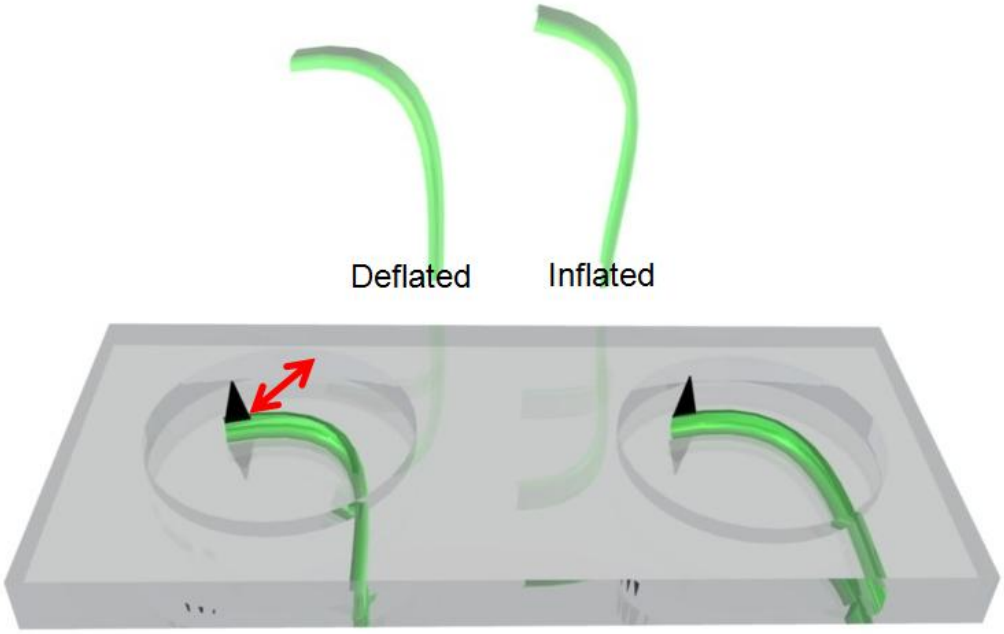


**Figure 9**: Bourdon tubes stretch in the plane when pressurized

Considering the ease of manufacturing planar bubbles, we devised mechanisms to sit atop the bubble layer and convert the direction of motion. We realized that two bubbles fitted would be able to tilt a horizontal cross-member affixed to them. By attaching a long vertical piece to the horizontal cross-

member, an arc would be traced along the skin, largely in the lateral direction. We also considered using bubbles that decrease in vertical height when inflated due to expanded cylinder diameter, depicted in Figure 10. In a later modification, we did away with the second bubble and considered making one end of the cross-member flexible, to be attached to the horizontal "ground" of the bubble plane. While these mechanisms all benefited from simplicity, we were concerned that amplification provided by the vertical member would not be adequate, and that manufacturing such structures on the millimeter scale would be problematic. Furthermore, using two bubbles to actuate one tilter would double the number of bubbles required.

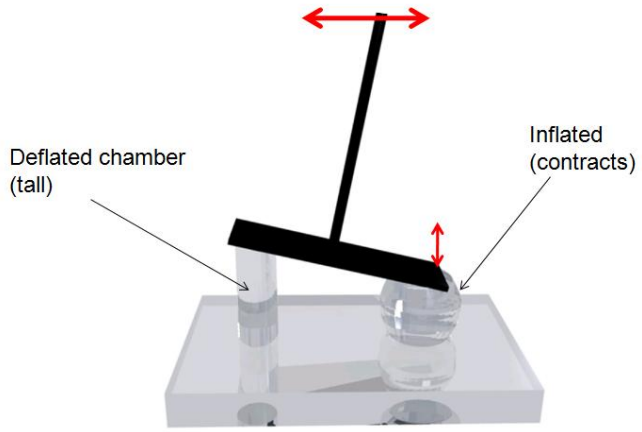


**Figure 10**: A tilting platform produces horizontal motion at the top of vertical attachment

Maintaining interest in vertical protrusions that rotate with bubble inflation, we also considered molding a layer of "hair" to be adhered on top of a plane of bubbles. As bubbles inflated, the ends of the hairs would diverge laterally, stretching the skin. After contemplating the compliance of thin animal-like hairs, we moved towards thicker stalks which could be readily molded but would not lose force in bending. An illustration of this concept is shown in Fig. 11. We hoped that the combined lateral stretch contribution of each adjacent stalk would combine to yield a significant overall stretch when applied. However the inherent compliance of any material which could be molded in one piece with a flexible membrane base was considered unacceptable. Furthermore, the addition of the additional membrane layer distributed over the bubbles would require more pressure for inflation.

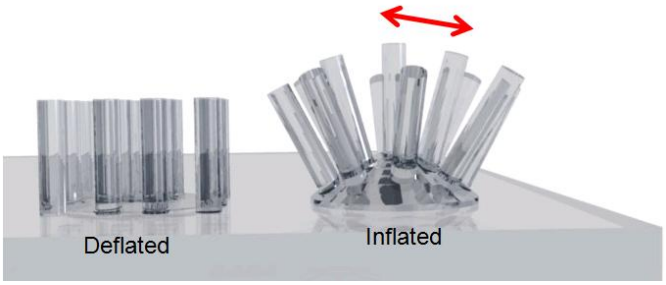


**Figure 11**: The inflated bubble spreads apart the protrusions that attached to it

**Fluidic Logic**
We considered numerous methods of channeling air within the display to better utilize space and minimize the number of electromechanical valves. In doing so, we reviewed pneumatic multiplexing and reviewed fluidic logic as discussed in detail in Appendix F. Our designs involving multiplexing could reduce the number of electromechanical valves, but would pose extreme manufacturing challenges and would prevent simultaneous actuation of arbitrary tactile displays.

## CONCEPT SELECTION

Our project involves relatively small-scale machining and components that our group has not previously worked with, so we found it difficult to apply any sort of scoring matrix to use our concept selection. In order to narrow down our tactile display design concepts, we decided to give the designs some perspective by machining some models out of acrylic (a potential material). We also researched relative topics in depth to understand all complications involved in the system. By doing this we were able to see which designs were feasible with our given resources and skill levels, which also led to slight changes in our design specifications. In the end, we found that perfecting a normally displacing pneumatic tactile array would first be required before designing a laterally actuated array and so we shifted our direction to normal displacement.

**Model Fabrication**
A machining resource that is readily available and very useful to us for our project is the laser cutter. We first used the laser cutter to machine models with holes of different diameter (0.5, 1, 2, & 3 mm) and engrave different width channels (0.5 and 1 mm) as seen in Figure 12. From this process we were able to depict that 0.5 mm diameter pneumatic bubbles were a little unreasonable due to their size. The 1mm bubbles seemed to be pushing our manufacturing abilities to the edge because we have to link a mechanism to the bubble to produce lateral motion. The model hole that seemed most applicable was the 2 mm, which allows for greater bubble displacement than 0.5 and 1 mm bubbles and it increases the number of different ways to link mechanisms to its motion, due to its larger surface area.

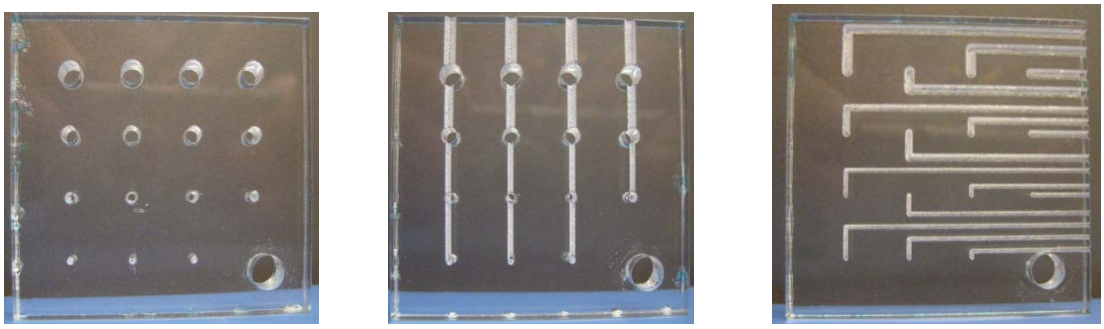

**Figure 12:** First model made with the laser cutter to help gauge sizes of channels and holes

The next step was to model a 4x4 array with 2 mm holes, 4 mm spacing center-to-center between holes, and 1 mm channels between holes as seen in Figure 13. This model shed some light on spacing issues involved with having a square array. The space in between holes is very limited in an inline array and this poses problems for linking mechanisms to each bubble. Another issue noticed was that channeling to holes in the center of the array tight and problematic. We addressed these issues by increasing the spacing between holes to 5 mm center-to-center and staggering the holes as seen in Figure 14. This approach allowed for greater working surface to the left and right of each hole and greater spacing for channels to the center of the array.

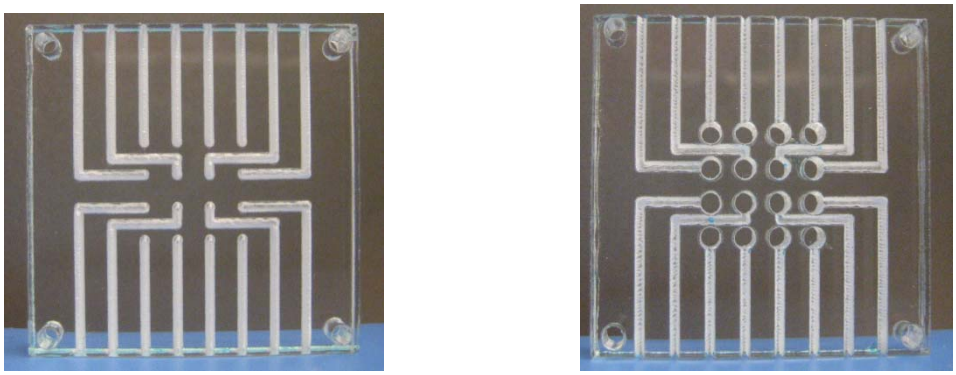

**Figure 13:** Second model made which indicated that square arrays have limited tactile spacing

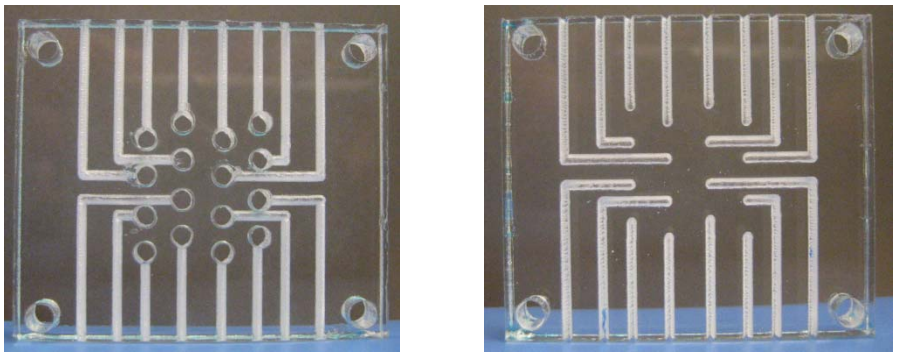

**Figure 14:** Last model made which showed a realistic tactile arrangement

The modeling also allowed us to better visualize the actual size of our designs and become familiar with possible manufacturing processes relevant to our project. This aided us greatly in recognizing design concepts that we just not feasible so we could dismiss the ideas and focus on more realistic designs. From the concepts above, we dropped the flexible membrane design due to it being hard to manufacture all the small protrusion cylinders and successfully mount them on a very thin membrane. We also noticed that manufacturing products in plane with layers is easiest when dealing with small applications, so both the sliding piston and sideways bubble concepts were also dropped. We decided to focus on a design similar to Figure 11, but to first develop the normally actuating bubble display due to increased complexity involved with creating a lateral mechanism.

Along with creating models out of acrylic, we tested the laser cutter's performance with another relevant material, PDMS as seen in Figure 15. We were able to burn a hole into the PDMS successfully and this opens up new manufacturing opportunities for us. We can now burn planar features into slabs of PDMS instead of dealing with complicated molds. The only drawback with laser-cutting the PDMS is that a burnt residue is left on the surface and this affects bonding of the PDMS.

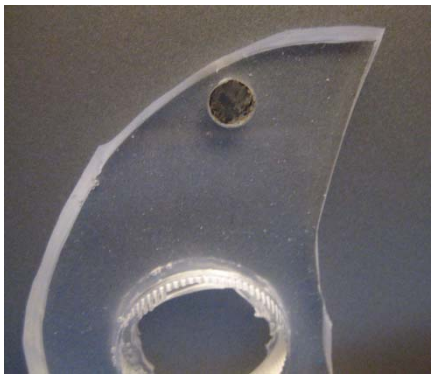

**Figure 15:** Test cut of the small upper hole using the laser cutter revealed its ability to successfully cut PDMS material

## FINAL DESIGN

Our final design (Fig. 16) contains all components of a functional system but focuses mainly on the tactile array, which consists of pneumatic bubble actuators and is fabricated out of polydimethylsiloxane (PDMS). The CO2 tank, valves, and tubing (upstream components) are standard manufactured equipment coupled together to power our tactile array. With the current design setup, the upstream components used are basic manufactured elements and are meant to be redesigned and made more compact at a later time.

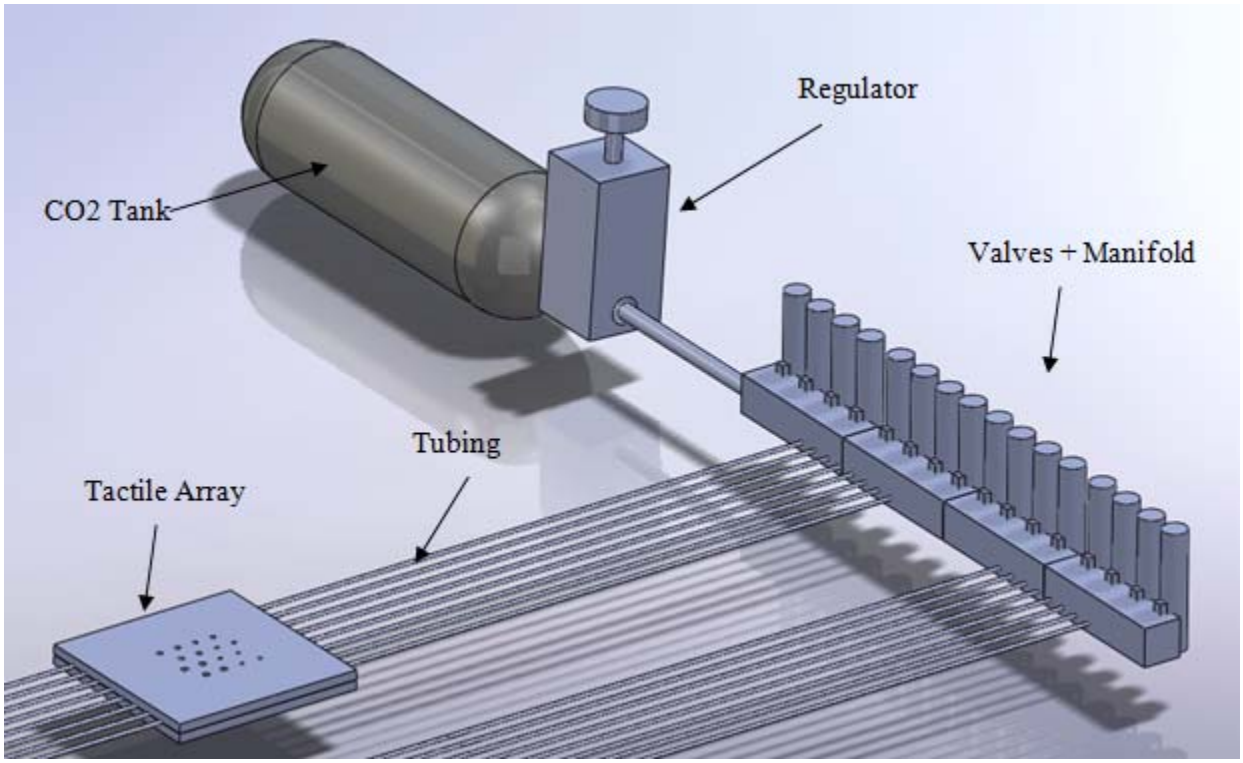


**Figure 16:** Final design of our system (tank, regulator, valves, and tubing only renderings and not the actual purchased components)

**Tactile Array**

Our tactile array contains 16 pneumatic bubble actuators which produce displacements normal to the top plane and are staggered in a 4x4 array as can be seen in Figure 17. The array is unique in the fact that there are four groups of different sized bubble actuators which have diameters of 1.00, 1.25, 1.50, and 1.75 mm as seen in Appendix A. The display consists of 3 layers (top base, bottom base, and thin membrane) which are all fabricated out of PDMS to allow the display to conform mildly to the user. The dimensions of the entire display are 50 x 50x 5.15 mm as seen in Appendix A. The two bases have pneumatic channels carved into them which are 0.25 mm in diameter are spaced 5 mm apart. The top base has through-holes at the end of each channel to connect the pressurized CO2 with the deflectable membrane.

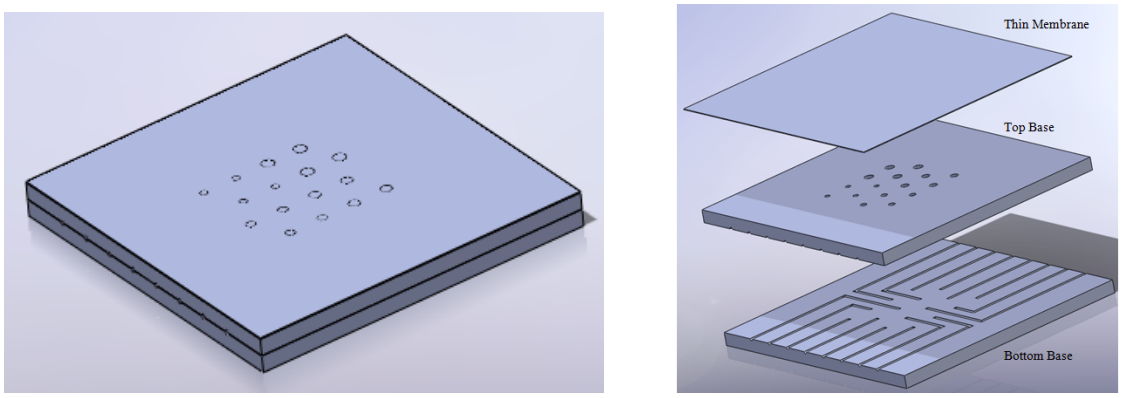


**Figure 17:** Tactile array with 16 different diameter bubble actuators

**Upstream Components**

The components that power our tactile array consist of a threaded high pressurized CO2 tank, regulator, and 16 three-way solenoid valves. The tank contains CO2 pressurized around 6900 kPa (1000 PSI), and the pressure will be brought down to around 200 kPa (30 Psi) with the aid of a regulator. The system will have standard solenoid valves with response times of 5-10 ms, which can operate at frequencies up to 100 Hz. The valves will be three-way so the pressure inside the actuating bubble can be normalized with the ambient air.

**PROTOTYPE**

We created a functioning prototype which differs slightly from the final design, as seen in Figure 18 below. The main difference is that the bubble diameters (Figure 19), which turned out to be 1.2, 1.4, 1.6, and 1.8 mm, are different than the designed diameters of 1.00, 1.25, 1.50, and 1.75 mm. This was due to manufacturing limitations and did not hinder the functionality of the prototype. Another difference was that we did not have a fitting to directly connect the small 0.5 mm tubing to the valve manifold and therefore had to step-down the tubing size with the aid of needles and barbed luer connectors. The last major difference is that the tactile pad is about double the thickness of the designed pad (5 mm) and this was also due to manufacturing limitations. The tubing-to-tactile pad interface was sealed with a silicone caulk which nicely matched the look and texture of the PDMS. However, this caulk did not provide the intended airtight seal as designed for and there were air leaks in a few channels of the tactile pad, but even with the leaks, the bubbles provided sufficient tactile stimulation to the users.

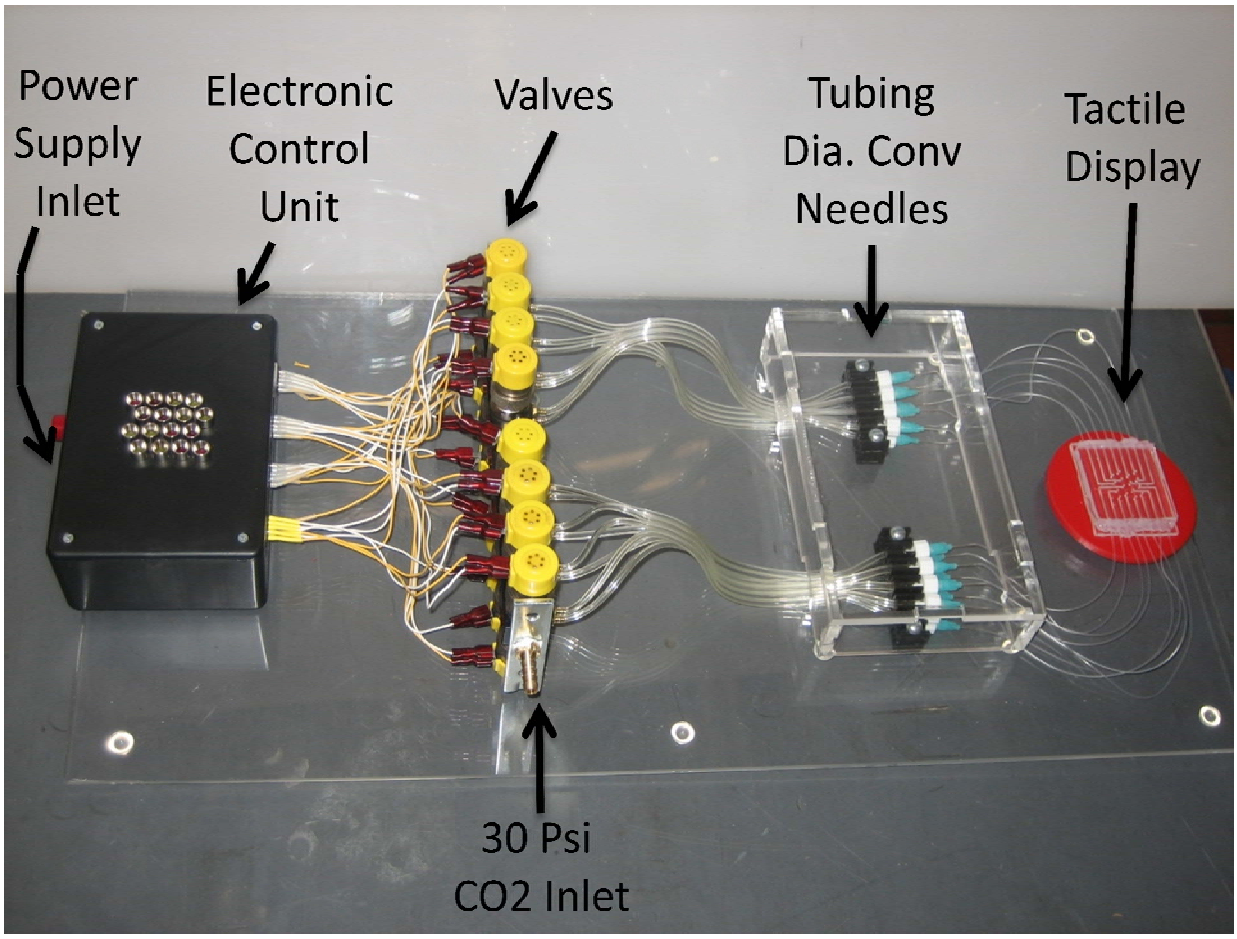


**Figure 18:** Prototype of our system (tank, regulator, and power supply not shown)

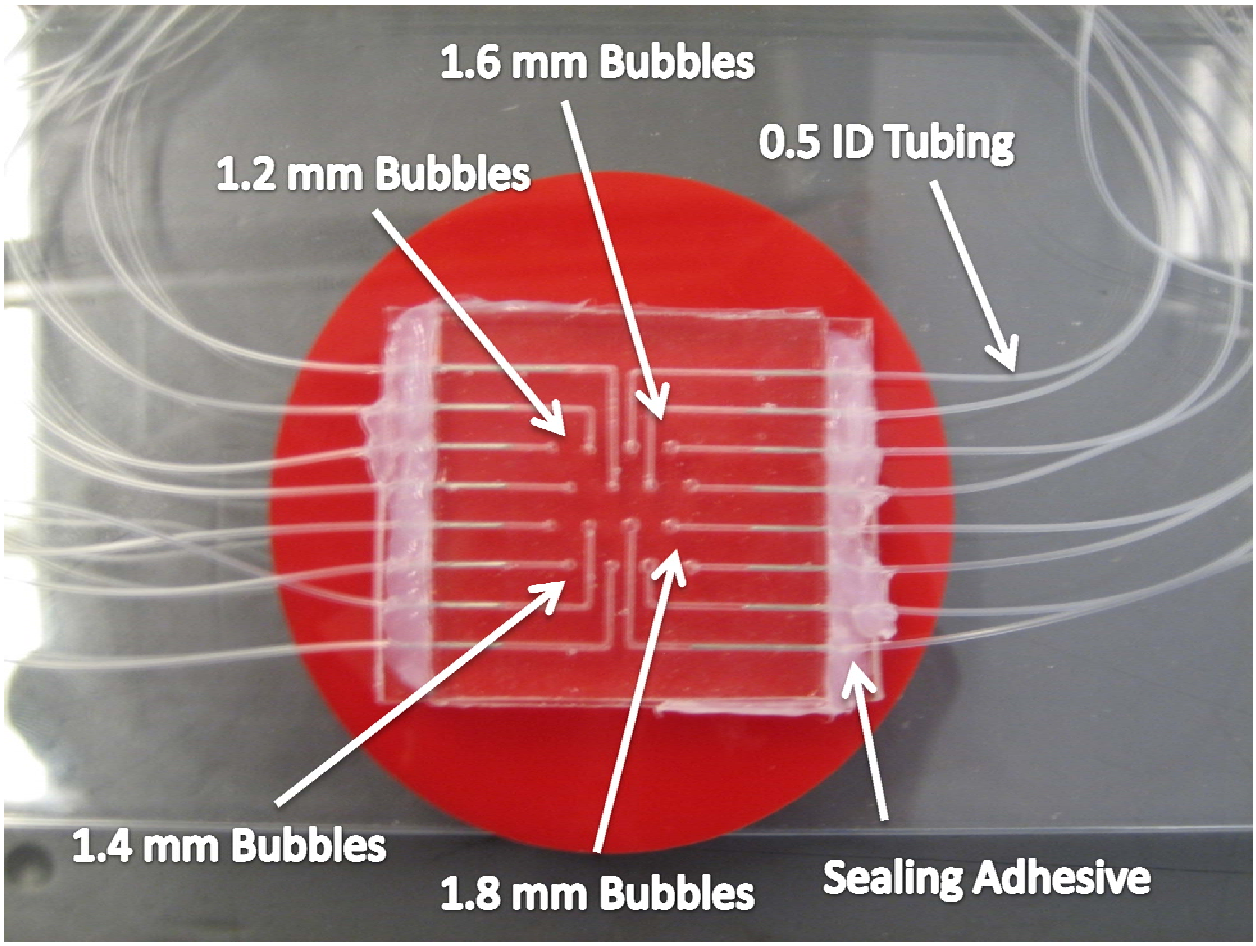


**Figure 19:** Zoom-in view of the tactile display with tubing attached

The electronic control unit contains a basic stamp microcontroller in the bottom of the enclosure and a printed circuit board is secured to the enclosure lid as shown in Figure 20. The microcontroller is powered independently by a 9V battery, where the printed circuit board is connected to a 24V power supply. The two components are connected by 16 signal wires which use to send control pulse from microcontroller to the circuit board for switching control of individual valves. A safety switch is available for immediate shut down in the case of emergency. The printed circuit board (Fig. 21) houses all the small electrical components such as transistors, resistors, LEDs (on the opposite side), four D-sub connectors. The D-sub connectors are used to organize the 16 electronically controlled valves.

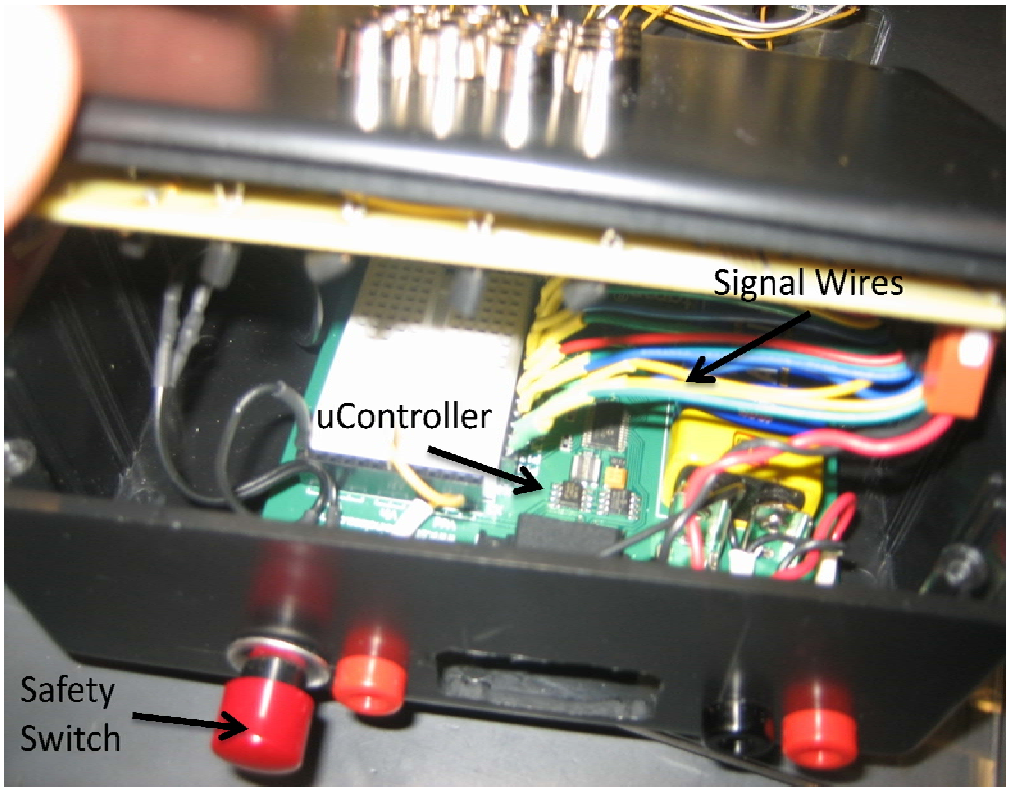


**Figure 20:** Internal circuitry with microcontroller,

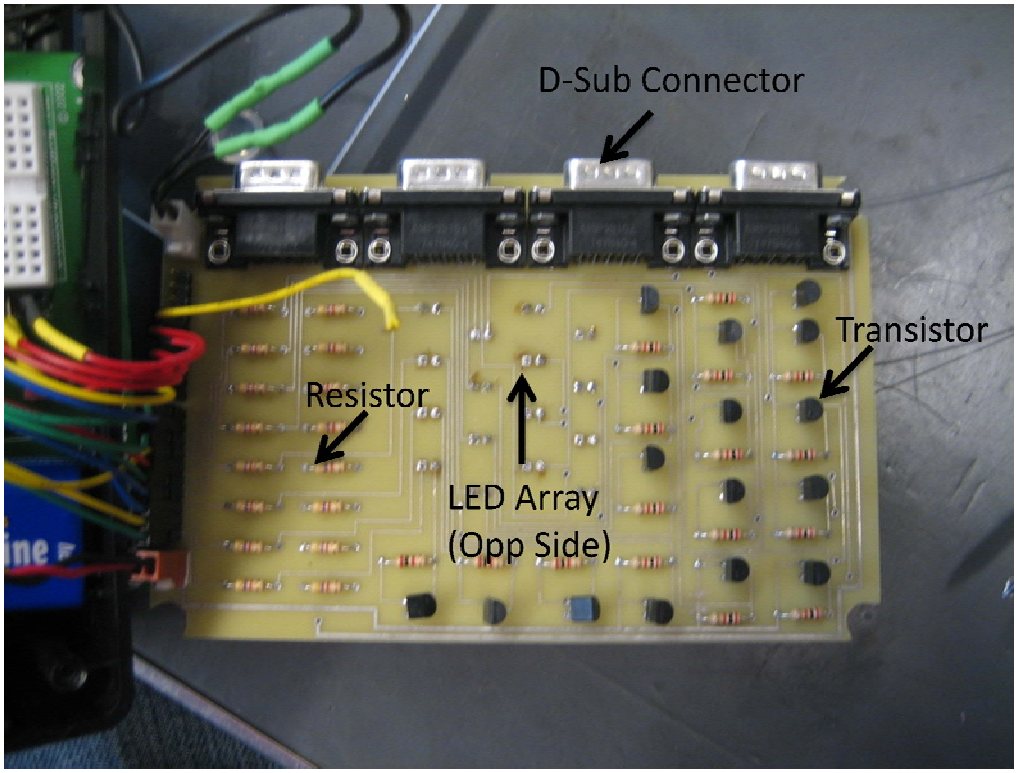


**Figure 21:** Printed circuit board which helped organize the 16 valve control circuit

**Prototype Critique**

Our prototype performed almost as expected during the whole design expo and allowed us to successfully test subjects, which was one of its design purposes. Each actuating bubble was perceivable and the array was durable enough to last through numerous trials with hard-handling subjects. The design does have flaws in the tube-array interface, top layer, and channel vibrations which could be addressed to provide for a more reliable design.

**Tube-array interface:** Although our prototype was fully functional, it did fail in the fact that there were a couple of air leaks at the tube-array interface, which lowered the force intensity of the actuating bubbles. These leaks were because the adhesive used to seal the interface (silicone caulk) allowed pressure leaks after repetitive pressure oscillations. While a better adhesive could just be used, a better design would be to implement a coupling tube into the molding process, which the PDMS forms around so no pressure loss occurs.

**Protective layer:** To accommodate typical use, another improvement would be to add a protective layer of a highly elastic or gel-like material over the thin PDMS membrane. While validation testing, a puncture occurred in the thin membrane causing one actuating bubble to stop working. This hole was caused by little force with a semi-sharp object which indicates the weakness of the membrane. A gel-like protective layer could have prevented this while mildly hindering the bubble performance due to its deformable nature.

**Channel vibration:** Due to the array base being made out of PDMS, the channels expand under pressure and cause vibrations on the pad which could interfere with the perception of the actuating bubbles. Addressing this matter could be done by making the channels more rigid which involves altering the elasticity of the PDMS during the manufacturing process. Another solution would be to minimize the expanding of the channels by increasing the thickness of the tactile array base.

## FABRICATION PLAN

Our tactile array (Figure 22) is the only component of our system that needs to be fabricated while the upstream components of the system just need to be assembled. We successfully fabricated a prototype tactile array which allowed us to create a feasible fabrication procedure. The first process in the fabrication plan is to fabricate the top and bottom bases of our array using polydimethylsiloxane (PDMS) which will be formed using a mold of machined aluminum. The next step is to use a plasma oven to bond the thin PDMS membrane to the top base and then bonded the top base to the bottom base together to form our tactile display. Next, hollow needles will be inserted into the channel ends, which will act as a coupler between the PDMS channels and polyethylene tubing. The needles need to be secured into place (airtight) with an adhesive. These processes are relatively simple but do require several attempts to completely fabricate a functioning product

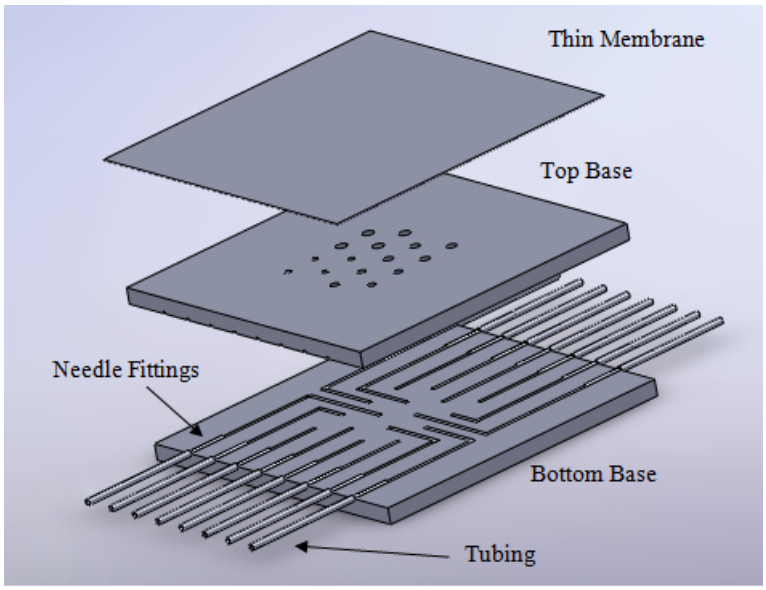


**Figure 22:** Exploded view of you tactile array which will be fabricated out of PDMS

**Creating the Bases**

There are a couple of different processes that can be carried out to fabricate the array as seen in Figure 23. The array is made out of a silicone elastomer (PDMS) and this material can be formed from a mold or a cured sample can be machined with a laser cutter. Based off of previous fabrication test attempts, we found that using a mold would produce the most functional sample so we decided to pursue molding. The setback with molding in our case was the difficulty to incorporate the bubble actuator through-holes into the mold. We then had to punch holes in the pad with sharpened hollow dispensing needles and this limited our bubble diameters to the inner diameter of the needles we could purchase, which turned out to be 1.2, 1.4, 1.6, and 1.8 mm.

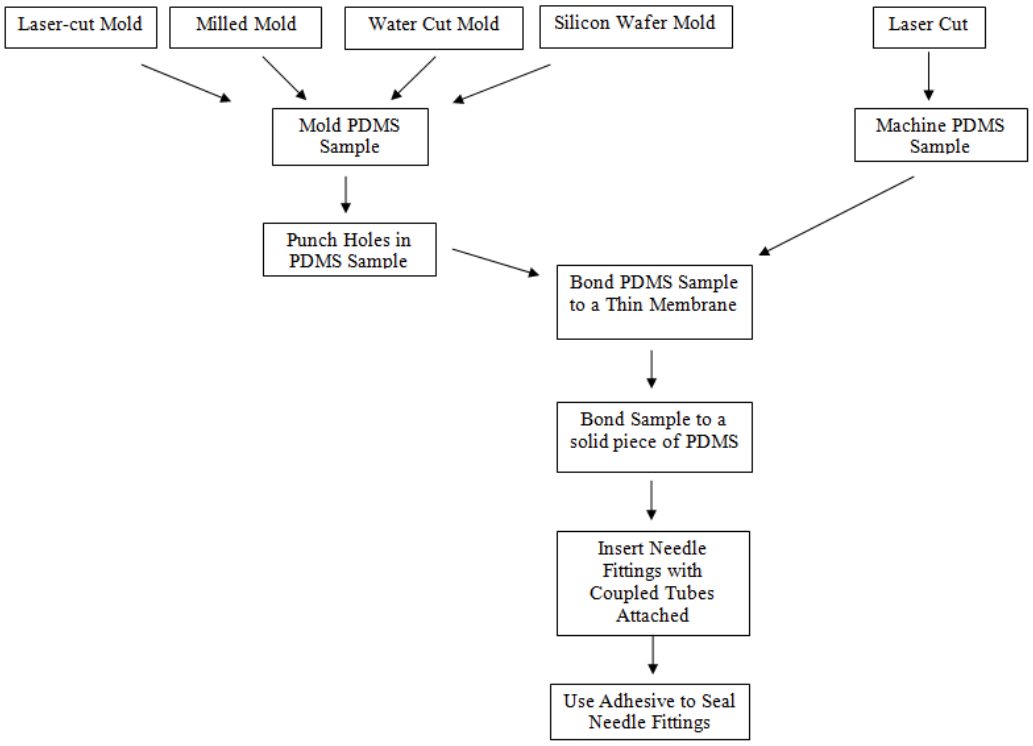


**Figure 23**: Possible fabrication processes to create the tactile array

**The mold:** We created a mold for our display out of 2 mm thin aluminum which was water-jet-cut into the shape of our interior channels as seen in Figure 24 below. The original design calls for a smaller channel; however, water-cutting a thinner piece of aluminum results in a distorted product. We followed this molding path based off of our previous manufacturing attempts, products seen below, and with the fact that our design features are much larger than features on traditional microfluidic devices, which typically use a silicon wafer mold.

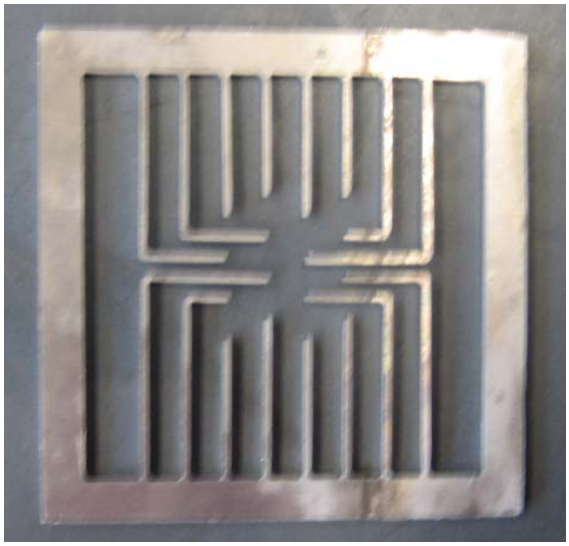

**Figure 24:** Water-jet cut aluminum mold for the channels

*The acrylic mold:* We fist attempted to mold the PDMS using a laser-cut acrylic mold, which provided insight on the difficulties of using acrylic and benefits of molding. The end product (Figure 25) was not a pretty sight, but it did have relatively good surface finishes and this greatly improves bonding success. Due to excess melting, the laser-cut acrylic mold's dimensions were not easily controlled and the cut channels were half as wide as we designed. Also, there is a lot of compliance with the very thin acrylic and this lead to inaccurate final features and breaking-off one of the channels in the molding process. On top of these difficulties, the acrylic was buoyant in the liquid PDMS, so additional efforts would have to be made to secure the acrylic down, which may alter our internal features.

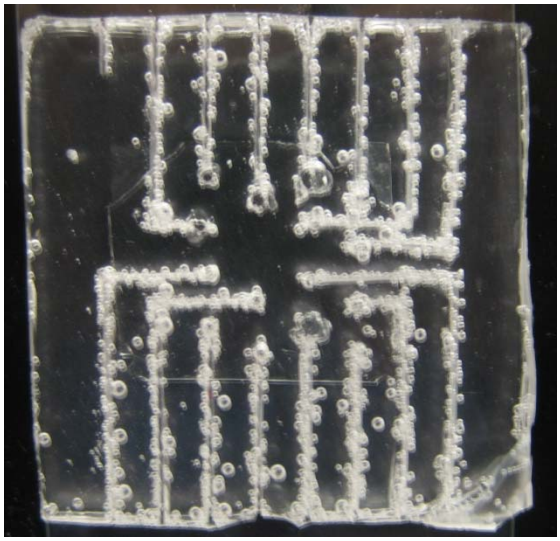

**Figure 25**: Molded sample with good surfaces but poor interior features

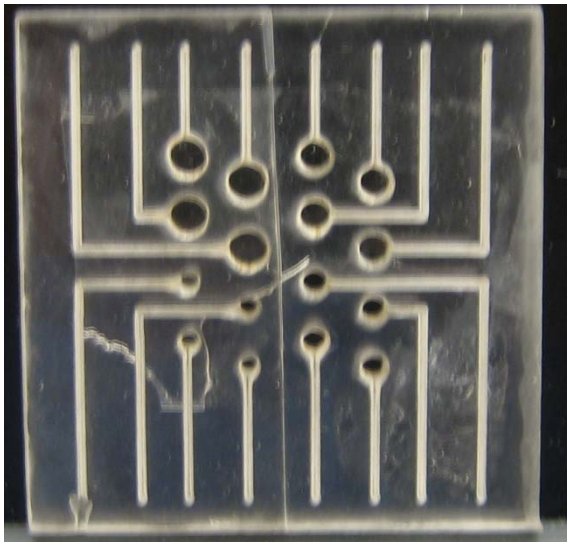

**Figure 26**: Laser-cut sample with good interior features but poor surfaces which effect bonding

*Laser-cutting the PDMS:* We also tried to machine a cured sample of PDMS with a laser cutter (Figure 26) and this produced relatively accurate internal features, however, excessive melting and burnt residue altered the surface finish of the sample. This made the sample almost impossible to bond to another surface and even with excessive cleaning; we did not have a high success rate.

**Creating the Thin Membrane**

We created the thin membrane by spinning liquid PDMS on a glass slide for approximately 30 seconds at angular velocities around 400 RPM and this resulted in membrane thicknesses of 0.12 mm. We found from several trials that it is a little difficult to remove the membrane when the thickness gets below 0.1 mm and therefore we found it best to work with membranes a little above that thickness. Using a silicon wafer as a base to spin the PDMS on is another method that may result in easier membrane removal, along with researching into some de-bonding agents. There are empirical formulas that relate desired PDMS thickness to angular velocity as seen in Figure 27, but we found these resulted in slightly inaccurate results and the process is easy enough to repeat until we obtain the correct thickness.

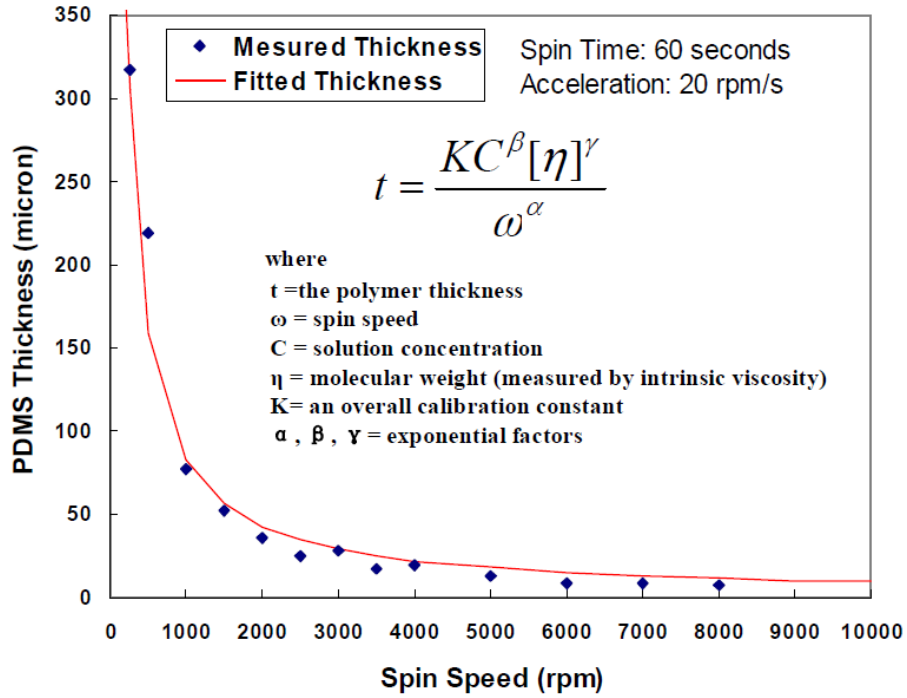


**Figure 27:** Empirical formula that relates spin speed to PDMS thickness [10]

**Bonding Pieces of PDMS**

We used a plasma oven to bond our top PDMS base to a thin membrane and then to bond the top and bottom bases together. After several attempts at bonding, we learned that a successful bond is directly related to surface quality and the strength of the plasma oven. This means that the less features (holes, channels, etc.) and foreign objects (dust, soot, etc.), the more successful the bond. This was apparent when the laser-cut samples, which had surface imperfections, rarely formed a good bond. We have been researching optimal PDMS bonding techniques which include cleaning surfaces with different solvents (isopropyl alcohol, acetone, and methanol) [11] in addition to our methods of cleaning the surface with soap and water. We also learned that the top base should be bonded to the thin membrane first and the bottom base second. This is due to increased difficulty of removing the thin membrane from the glass slide when the piece being bonded to it is too stiff.

## SYSTEM ASSEMBLY

Our system (Figure 16) can be broken down into a mechanical and electrical assembly, both of which are relatively simple. The design emphasis was on fabricating the tactile pad, which has much complexity, while the rest of the system is a simple arrangement of manufactured parts which fit together with little difficulty.

**Mechanical Assembly**
The mechanical assembly consists of attaching the tank to the regulator, tubing to the regulator, tubing to the valve manifold, tubing to a needle fitting, and needle to the tactile array as seen in Figure 28 below. Our design involves directly connecting the small 0.5 mm ID tubing to the valve manifold with an appropriate fitting; however, we connected 1.5 mm ID tubing directly to the manifold in our prototype and this required a tubing diameter-drop sub-system as seen in Figure 29 below.

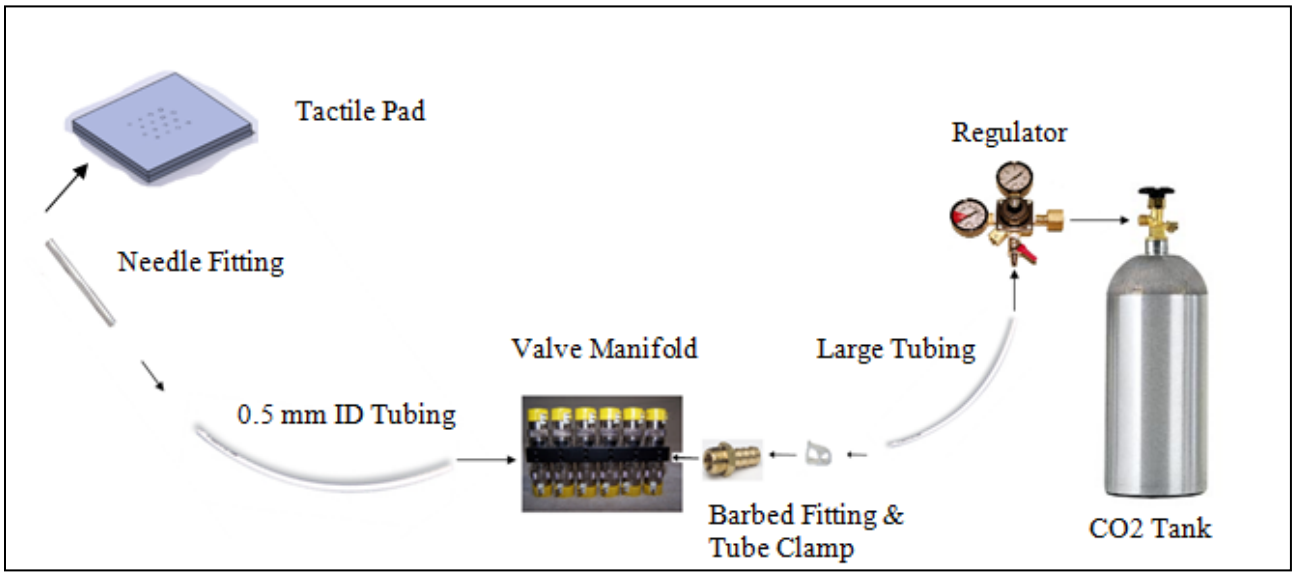


**Figure 28:** Mechanical assembly of our designed system

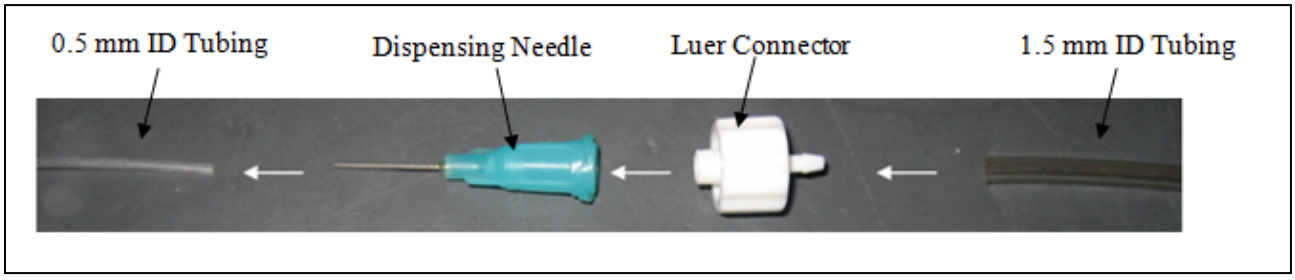


**Figure 29:** Prototype tubing diameter drop assembly (differs from final design assembly)

**Electrical Assembly**
The electrical assembly of our system consists of connecting our valves to a circuit board, a power supply to our circuit board, and our circuit board to a micro controller. The circuit board used was printed and the components (resistors, transistors, LEDs, etc) were soldered onto the board, schematic seen in Appendix A. The valve wiring was organized using 9 pin D-Sub connecters, which connected directly to the circuit board.

## BILL OF MATERIALS

We created a functional tactile array system prototype for around $620 as can be seen in an abbreviated bill of materials (Figure 30) below, while a complete version is located in Appendix E. For out prototype and our design, the upstream components of our system (electrical components, valves, tubing, and fittings) cost the most money. This does not include any cost for the CO2 tank or regulator because they

were borrowed for the duration of the project. The tactile pad components (small tubing, needle fittings, and PDMS) were relatively cheap compared to the upstream components and this fact provides a driving force to concentrate research on improving upstream components.

| Component | Quantity | Total |
|---|---|---|
| Small Polyethylene Tubing | 6 m | $55 |
| Sylgard 184 Silicone Elastomer (PDMS) | 0.5 kg | $73 |
| Ribbon Tubing | 1 m | $9 |
| Standard Solenoid Valve (used) | 47 | $78 |
| Needle Fittings | 50 | $14 |
| Borrowed CO2 regulator | 1 | $0 |
| Borrowed 5 lb C02 Tank | 1 | $0 |
| Printed Circuit Board | 1 | $95 |
| Basic Stamp Controller | 1 | $95 |
| Various Electrical Components | N/A | $96 |
| Various Manufacturing | N/A | $53 |
| Various Assembly | N/A | $52 |
| | **Grand Total** | $620 |

**Figure 30:** Abbreviated bill of materials for our system indicates cost of prototype production to be around $620. The majority of the expenses are due to upstream components.

## ENGINEERING ANALYSIS

All of our proposed concepts involve fairly complex pneumatic networks involving electrical valves that drive an array of tactor mechanisms. Our analyses follow from the functional decomposition described in Figure 5, and include valve control, the bubble-skin system mechanics, pneumatic loss analysis, and a materials comparison.

### Valve Control

Our research indicated that frequency has significant impact in terms of human finger perception performance. Therefore, it is crucial for us to be able to operate the valves in a wide range of frequencies. A basic flow chart of our valve control system is shown in Fig. 31.

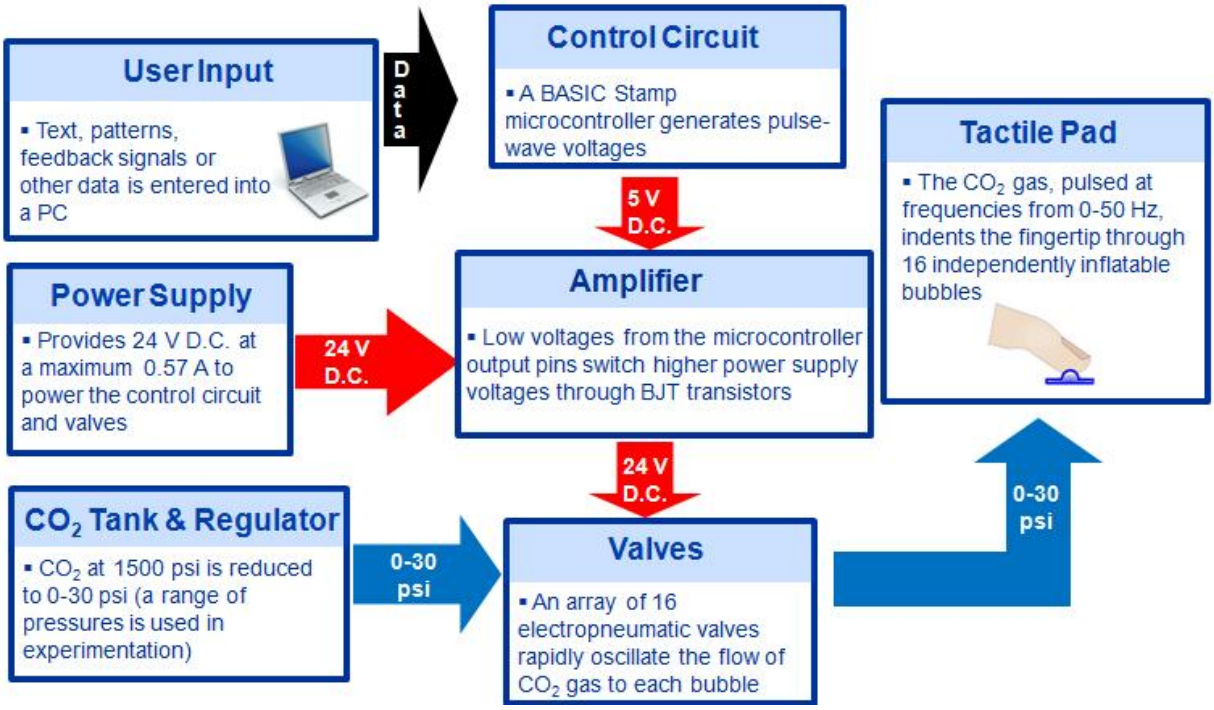


**Figure 31:** Valve System Flow Chart

The valves used in this project are standard Clippard 3-way 24V valves. The valves are controlled by basic stamp microcontroller that could be operated at frequency range from 0 – 100 Hz. The frequency control is done by pulse width modulations outputted by the microcontroller. We have written several programs in BASIC to perform simple two point discrimination tests. Between the microcontroller and the valves, there is a custom printed circuit board that we designed to integrate all electrical components in a much more organized manner, such that we could place all the components in a project enclosure. The layout of the printed circuit board could be found in Appendix A.

Initially, we plan to obtain a high performance Lee valve that would capable of reaching 200+ Hertz, and that will allow us to explore the characteristic of other human finger perceptual mechanisms at the high frequency domain. However, we were not able to obtain the Lee valve due to its long lead time.

The printed circuit board houses all the switching control circuit for the valves. The basic layout of individual switching circuit is shown in Figure 32, and the entire switching schematic could be found in Appendix A. It is composed of a NPN transistor and two resistors for manipulating base current to ensure the transistor switches properly. The valve is modeled as a variable resistor based on the specification that its resistance varies with voltage and current. Using the large signal model, we are able to calculate the based current base on the two resistor's values and therefore should be able control the collector current that flows through the device using Equation 1 below.

$$I_c = I_b \times B_f, \quad B_f = 75\ (typical\ current\ gain) \tag{1}$$

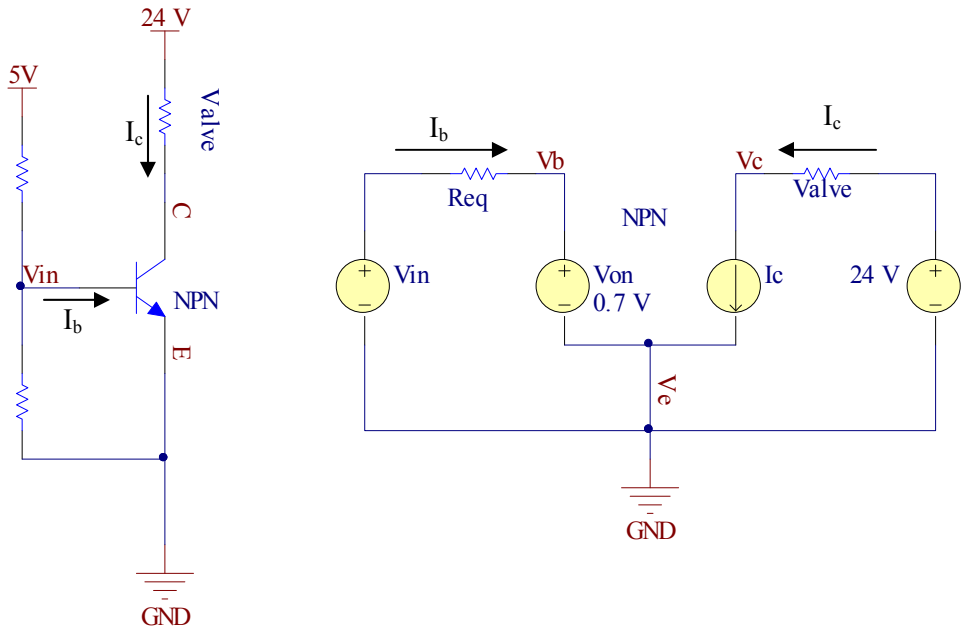


**Figure 32:** Single Valve Control Schematic

A simple 4 x 4 LED array is also housed on the printed circuit board and extruded through the enclosure lid to provide a visual representation of the tactile display for demonstration purposes. The LEDs are directly power by the microcontroller signal.

With the use of printed circuit board, the circuit is kept as simple as possible so that future groups could spend less time on realizing this part of the project and will focus on the main objective, the tactile display.

Based on our measurements, the power consumed by the valve switching operation is approximately 15 Watts. Therefore, there is still room for major improvement on minimizing the power consumption of the valve switching operation and increased the overall efficiency of our device in the future.

**The Bubble-Skin System Mechanics**

Our tactile array uses inflatable elastomeric membranes with circular boundaries, i.e., bubbles. The bubbles inflate to convert air pressure to mechanical displacement of the fingertip skin. We analyzed the bubble-skin system in order to optimize skin displacement within manufacturing constraints and to compare available displacements to perceptual thresholds.

As gas pressure inflates the bubble against the skin surface, a blocking counter-pressure due to the skin's elasticity works in the opposing direction. To predict the displacement of the skin, a model incorporating both the elasticity of the bubble and the skin is required. We used a lumped element model, treating the bubble as a nonlinear spring in extension. The fingertip skin was modeled in compression, having a frequency-dependant spring constant. The force F deflecting the system was found by multiplying the gas by the circular face area of the deflated bubble. As the bubble is fixed to the tactile pad, it was treated as having one fixed end. The skin element was also considered to have a fixed end, as the motion of the finger itself is negligible due to its relatively large mass and stiff joints. The free ends of the two elements thus shared a displacement x. Figure 33 shows the model we used to analyze the system.

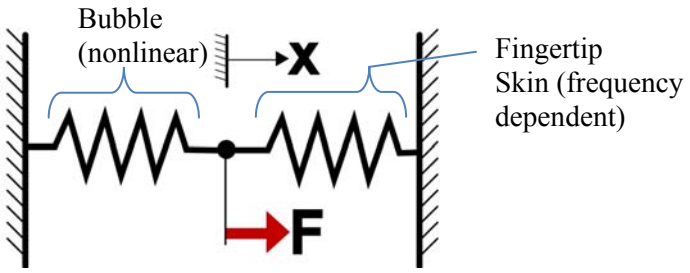


**Figure 33**: The force generated by gas pressure is resisted by the elasticity of both the bubble material and the fingertip skin.

To model the bubble as a nonlinear spring, we used plate theory to relate bubble tip displacement to bubble pressure. Using circular bubbles with fixed boundaries simplifies the governing partial differential equations used to model flexible membranes under uniform pressure, resulting in Equation 2 [12], where bubble tip deflection $\delta$ depends on the bubble radius $r$, applied uniform pressure $P$, Young's Modulus $E$, and membrane thickness $t$. This equation has been used previously by MEMS researchers ([13], [14]) to predict the displacement of PDMS bubbles.

$$\delta = 0.662r\left(\frac{rP}{Et}\right)^{1/3} \tag{2}$$

Modeling the fingertip skin under oscillatory load is a challenge as it understood to be a viscoelastic material, combining the properties of elastic materials with the time-dependent properties of viscous fluids. Several prior approaches have used Fung's Model, a widely-used viscoelastic tissue model, to analyze the fingertip displacement under normal loads from small indenters. Pawluk and Howe [15] used empirical testing of a fingertip under load to find corresponding parameters for a single-element application of Fung's Model. Later Wu et al. [16] used a finite element approach based on Fung's Model to predict the fingertip's response to a vibrating point indenter. While these models showed promise in predicting the skin' response, we chose to model the skin by directly applying experimental results obtained by Dong & Srinivasian [1], who used a 0.7 mm cylindrical fingertip indenter with sinusoidal displacement from 0 to 100 Hz to test the force vs. displacement relationship of the skin. We used the force-displacement results obtained by Dong & Srinivasian [1] for a set of eight frequency values from 1 to 56 Hz to represent a spring constant for the finger at each corresponding frequency.

Since our model assumed that the bubble and finger shared a displacement, we converted the pressure in Equation 2 to force and then equated that force to the each of the forces obtained empirically by Kyung to obtain a set of equilibrium force-displacement relationships. By examining these equilibria, we can predict the minimum pressure needed to obtain a given displacement at a selected frequency. Fig 34 shows, for a 1 mm diameter bubble, a zone of equilibria representing possible intersections between the nonlinear bubble force at the range of thicknesses under consideration and the blocking force of the skin at the range of frequencies under consideration. In combining the frequency-dependent experimental results with our frequency-independent bubble model, we note that the experimental results provide a peak displacement corresponding to maximum force amplitude. Since the first resonance of the bubble is expected to be far greater than the 0-30 Hz range of operating points, we model it as a static mechanism and do not consider the contribution of its energy storage properties.

At the minimal film thickness and maximum frequency, our approach indicates displacement will be greatest. Figure 34 also shows the threshold of perception for normal displacement [5], indicating that our proposed parameter ranges result in displacements that handily exceed perceptual thresholds (the thresholds are very slightly frequency dependent, which is not apparent in the figure due to the scaling).

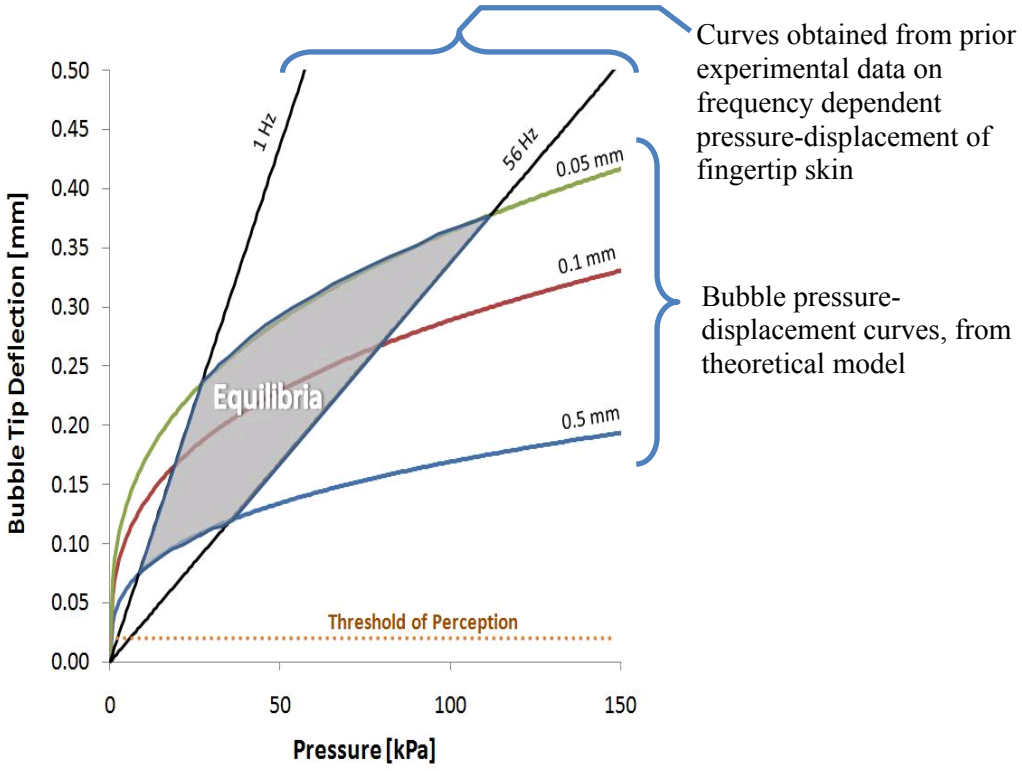


**Figure 34**: For a 1 mm diameter bubble, the space of equilibrium operating points is found at the intersections of curves representing elasticity of the bubble and fingertip skin

Figure 34 shows a range of displacements for a fixed bubble radius. Noting the strong dependence in Equation 2 on radius, we present another range of bubble-skin system displacements in Figure 35, where the frequency is fixed at 56 Hz, corresponding to the maximum shown in Figure 34. The sharp peak in displacement shown in the range of 0 to 0.1 mm membrane thickness is notable.

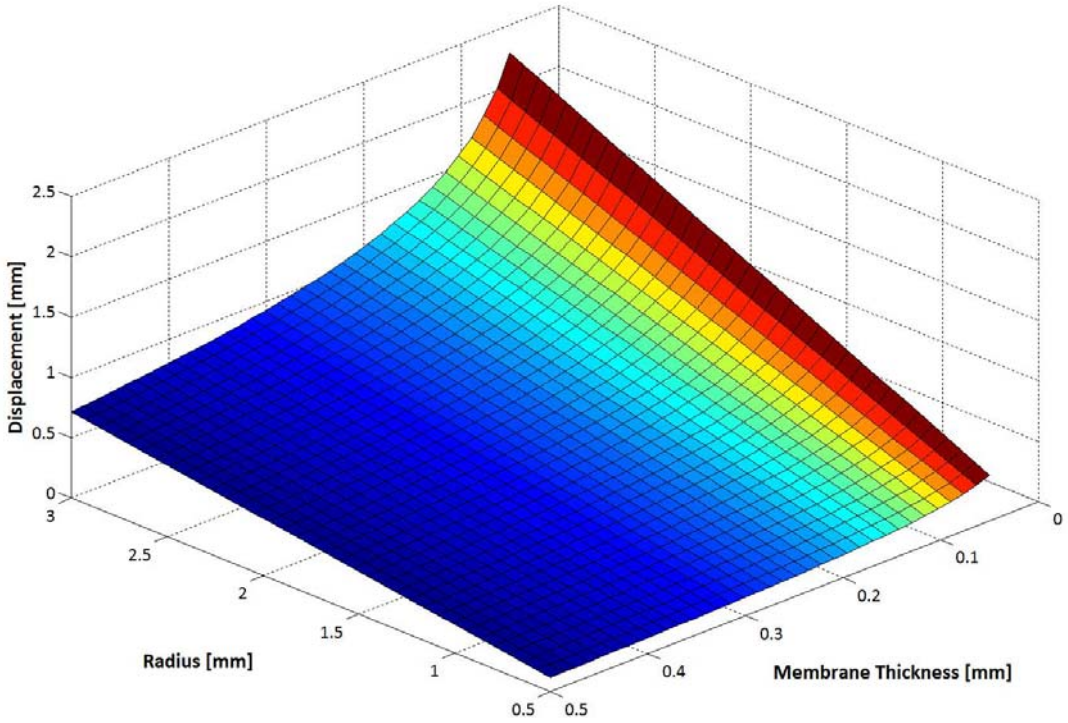


**Figure 35**: With frequency fixed at 56 Hz, the skin displacement is shown as a function of bubble radius and membrane thickness. Keeping the membrane between 0 and 0.1 mm strongly affects displacement.

We note that in applying the empirical results obtained by Dong & Srinivasian [1] to our skin displacement model, we are assuming direct similarity of their experimental setup to our tactile display. The indenter used by Dong & Srinivasian was cylindrical but not rounded like our bubble, which may compromise the above analysis. The shape of the indenter affects local stress fields, which affects the response of those mechanoreceptors (Merkel Discs and Meissner Corpuscles) which our display seeks to stimulate. Merkel discs are used in sensing textures and are believed to be quite sensitive to skin curvature. Our analysis confirms that our proposed pressure ranges are adequate for producing the desired displacements, and demonstrates the advantage of using very thin membrane thicknesses.

**Pneumatic Losses**

Pneumatic networks can in principle be analyzed using the theory of compressible flows in closed channels, and by computational fluid dynamics (CFD) simulations. In practice, we found the available theory helpful for qualitative analysis only in developing our first design, due to the unavailability of developed models and empirical constants applicable to our novel geometries (for several needed pneumatic components, adequate flow properties are not supplied by the manufacturers). We also avoid investing time in CFD simulations due to the inherent complexity of our system, and consider physical bench testing of a single-tactor test cell as adequate for first round testing.

Our prospective designs all utilize a regulator to drastically reduce the pressure and flow output from a high-pressure air reservoir, so we assume the ability to dial up an essentially arbitrary pressure at the system input. Our concern then is with the frictional head loss due to the narrow diameter tubing used and additional losses due to fittings, valves, and the internal geometry of the tactor pad. If these losses are large, a resulting low flow rate will increase the rise time to inflate the bubbles, dissipating energy and limiting the frequency at which tactors may be actuated. We know that increasing the diameter of our tubing, fittings, and valves will result in less frictional resistance to flow, but our intuition is that the

ability to prescribe input pressure will allow us to manually adjust the regulator to obtain the necessary bubble inflation rise time using the small pneumatic components and narrow tubing we have identified so far.

Our current tubing system from the exit of the valves to the individual bubble consists of four different lengths and diameters, as seen in Figure 36, so there will be frictional energy losses due to the flow of the fluid.

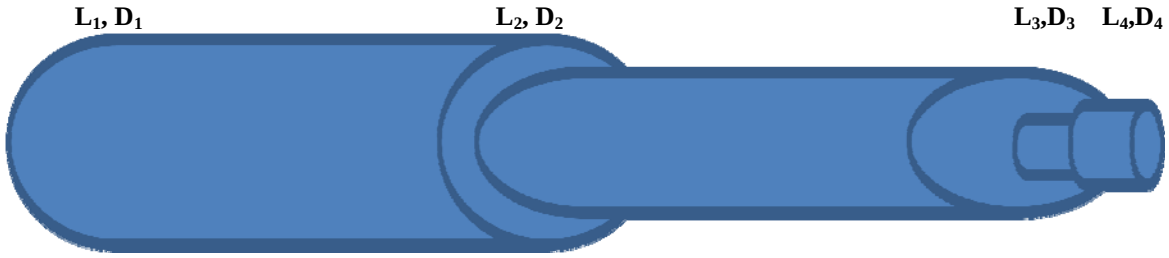


**Figure 36**: Current Tube Connection

The flow is expected to be a transient and unsteady flow with velocity and pressure change over time. The fluid is also compressible as its density change with pressure and we cannot neglect the internal energy during the flow. Unpredictability occurs during operation where the tubes' shape will be constantly changing and it will account for minor head losses. We analyzed the nature of our flow whether it is laminar or turbulent using the Reynolds number. Assuming incompressible, streamlined flow at the instantaneous entry point with 30 psi (≈200kPa), we applied the Bernoulli's equation (Equation 3) to obtain the entry velocity and calculate the fluid's Reynolds number (Equation 4) and it was much larger than critical Reynolds number of 2300 which make our flow a completely turbulent flow. Based on the condition of our flow, it is nearly impossible to have a complete and accurate analysis without further experiments.

$$V = \sqrt{(2\frac{P}{\rho})} \tag{3}$$

$$Re = \frac{\rho V D}{\mu} \tag{4}$$

The overall head loss for the system consists of losses due to viscous effects, $h_{L\ major}$ (Equeation 5) and losses in the various tube components, $h_{L\ minor}$. (Equation 7). Major losses take into account the friction factor, *f*, where *f* is a function of Reynolds number, *Re,* equivalent roughness, $\varepsilon$, and diameter of the tube, *D* as shown in Equation 6. For a completely turbulent flow, *f,* is independent of the Reynolds number and $\varepsilon$ is zero for smooth plastic tube. However, *f* is not zero even for a smooth surface as the no-slip boundary condition that requires any fluid to stick to any solid surface it flows over.

$$h_{L\,major} = f\,\frac{l}{D}\frac{V^2}{2g} \tag{5}$$

$$f = \Phi(Re, \frac{\varepsilon}{D}) \tag{6}$$

The minor losses occur due to additional components such as bends, tees, or tangles which will inevitably occur during the operation of our system. Minor losses depend on the loss coefficient ($K_L$) shown in Equations. 7-9, which is a function of area and geometry of the tube.

$$h_{L\,minor} = K_L \frac{V^2}{2g} \tag{7}$$

$$K_L = \left(1 - \frac{A_1}{A_2}\right)^2 \tag{8}$$

$$K_L = \Phi(Geometry) \tag{9}$$

We want to minimize the energy loss in our system by changing the factors that we can control. Major losses are proportional to *l/D* so we want to make our tube as short and as large as our constraints allow. Minor losses are affected by geometry and area change of the tube. The geometry is impossible to predict as our tubes do not have a fixed position so we will minimize minor losses by having as few area change as possible.


**Figure 37**: Optimal Tube Connection

**Materials Comparison**

The tactile display uses pneumatic actuation to create a stimulation on the skin, based on our specifications, the materials involved have to be inert, non-toxic, readily available, can be manufactured to millimeter scale and reasonably priced. We have research several materials to be used for our display which includes the body structure and the bubble membrane (Table 3) and have decided to manufacture our tactile pad almost completely out of polydimethylsiloxaen (PDMS). This decision was based on the molding, elastic, and bonding prosperities of the material as described below.

**Polydimethylsiloxane (PDMS)**

PDMS is the most commonly used silicon based polymer, an elastic material which has the ability to form reversible and irreversible seals. The irreversible seal can be made by bonding the two pieces of PDMS under Plasma oven and this is important since we need to bond our base, channel and membrane together. Although this bonding process is simple, the surfaces of PDMS have to be cleaned thoroughly and as the features on the surface increase, the less successful is the bond [14]. The fabrication of PDMS is straightforward and it can be cast against a suitable mold with sub-0.1-μm fidelity [14] which makes it suitable to be used in the microfluidic system such as ours. It also has a low surface energy ~ 20erg/cm$^2$ [14] so it can be released easily from molds. PDMS also has insulating thermal properties so it does not allow dissipation of heat and can be used to insulate heated solutions or gases. The elastic properties with Young's Modulus of ~ 750 kPa [14], which can be changed based on the base-to-curing agent ratio, allow for surface conformity and facilitate release from molds. PDMS is non-toxic and has been used extensively in the biophysical application.

| | Acrylic | Epoxy | PVC | PDMS |
|---|---|---|---|---|
| Density (lb/in$^{3)}$ | 0.0426 – 0.0434 | 0.0506 – 0.0614 | 0.0455 – 0.0488 | 0.0368 - 0.0441 |
| Price (USD/lb) | 1.14 – 1.25 | 9.32 – 10.3 | 0.907 – 0.998 | 5.86 – 6.45 |
| Yield Strength (ksi) | 8.4 – 9.24 | 32 – 40 | 4.76 – 5.25 | 1.02 – 1.67 |
| Tensile Strength (ksi) | 10.5 – 11.5 | 40 -50 | 6.4 – 8.7 | 1.02 – 1.67 |
| Operating Temperature (°C) | -70 - 120 | -90 - 180 | -50 - 80 | -50 - 200 |

**Table 3:** Material properties of considered materials in our tactile display[17]

## DEVICE TESTING

### Psychophysical Testing

As our tactile display is meant to convey information to human beings, it was necessary to further verify its performance with human subjects. We recruited nine volunteers at the University of Michigan 2009 Design Expo. The LED display was covered and subjects were asked to identify the number of bubbles actuated while we used our control software to execute the test sequence shown in Table 4. The test sequence actuates bubbles within each of the four quadrants corresponding to bubble diameters designed into the pad. The groups of bubble diameters were tested in the following random order: 1.4 mm, 1.2 mm, 1.8 mm, 1.6 mm.

| Bubble Diameters [mm] | Test Sequence |
|---|---|
| 1.2 | 2,1,4,3 |
| 1.4 | 1,3,2,4 |
| 1.6 | 3,1,2,4 |
| 1.8 | 3,1,4,2 |

**Table 4:** Within each bubble diameter quadrant, a test sequence was executed. The number 1-4 indicate how many bubbles were simultaneously activated.

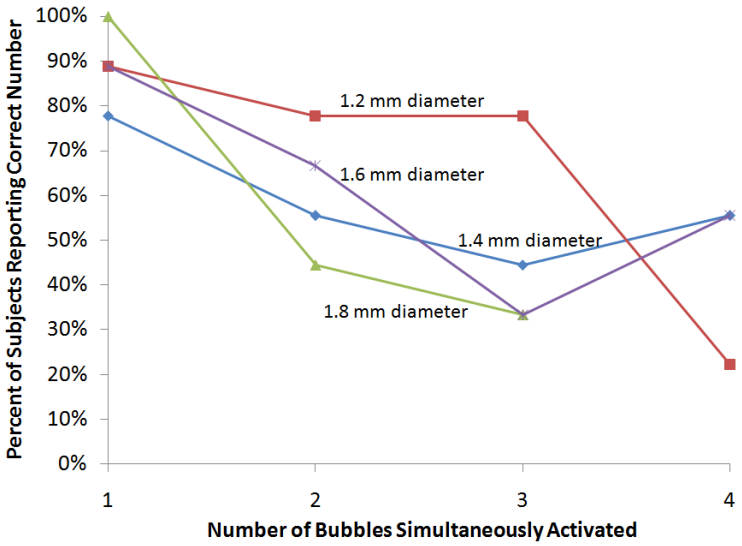


**Figure 38**: Subjects correctly reported the number of activated bubbles best when the diameter of the bubbles was smallest (the lines connecting data points are for graphical clarification only).

The results, shown in Figure 38, indicate that subjects had increasing difficulty identifying the number of activated bubbles when the number activated increased. The smallest diameter bubble tested, 1.2 mm, had the highest overall number of correct responses, indicating that a smaller bubble produces an effect that is sharper and easier to perceive. Further testing is warranted, however, as our models indicate a smaller skin displacement with decreasing bubble diameter. While shrinking the bubble further may sharpen the perception, eventually the bubble would not be perceived as it would fail to meet vertical displacement perceptual thresholds.

Further testing is also appropriate due to the small number of subjects used (n=9) and possible confounding variables. The valve switching noise was clearly apparent, and some subjects may have been able to audibly infer the number of bubbles activated from valve sounds. We also expect that improved performance would be observed with a series of training rounds, as subjects were somewhat startled by the new perceptual experience and may perform better after becoming familiar with the sensation.

**Physical Testing**

We performed a preliminary physical test to measure the bubble tip displacement and the bubble radius of our display using a digital vernier caliper with a resolution of 0.01 mm. The results were plotted with theoretical values from plate theory where we model the bubble as a nonlinear spring [12] as seen in Figure 39. For this test, the pressure of the bubble was set at static pressure of 20 Psi.

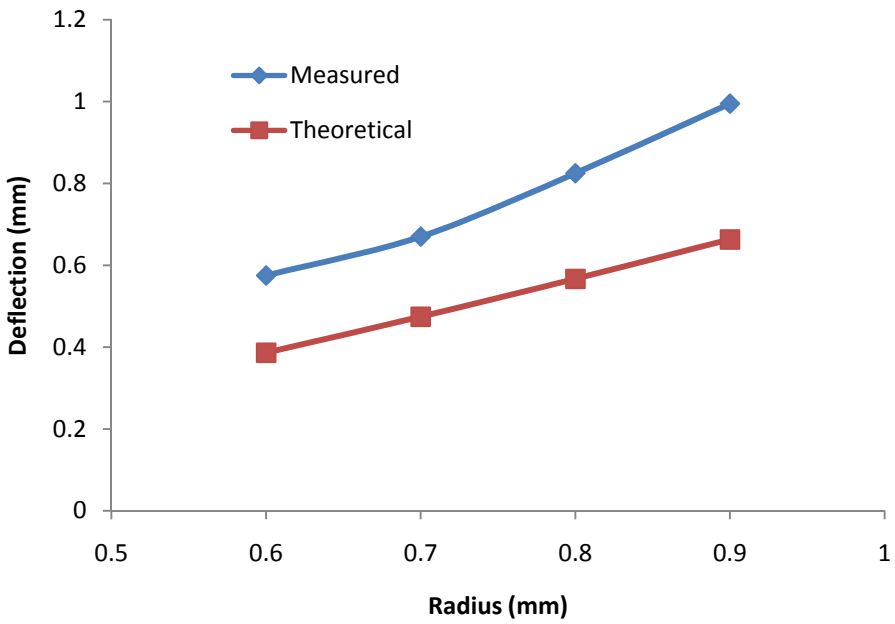


**Figure 39:** Comparison between measured and theoretical values of bubble defection indicate around a 30% difference

From the figure, the deflection increases as the bubble radii get larger and our measured data show similar trend but the measured bubble tip displacement is significantly larger than the theoretical values by roughly 30 %. The test we performed had many variables due to the testing methods used which involved eyeing the bubble displacement with calipers. This difference in displacement needs to be further explored with additional future testing as mentioned below, but it does provide a rough correlation between the actual and theoretical values of free bubble displacement.

**Future physical testing:** More physical testing remains for future work. To measure bubble tip displacements, an optical measuring microscope equipped with a z-stage measurement system can be used, which uses image processing software to measure vertical displacements from focus properties. To optically isolate the bubble tip for analysis, pinhole attachments can be used. The software will allow measurement of the tip displacement while the bubbles are oscillating. The microscope's reticule can be used to measure bubble diameters in the x-y plane, allowing for verification of the accuracy of our manufacturing methods. To measure force output,  a piezoelectric load cell can be used.

## RECOMMENDATIONS

After producing a working prototype, we would have obtained a great deal of knowledge in successful manufacturing techniques and in future design directions that show great potential. This knowledge will help steer future research in directions that will be most beneficial and save valuable time avoiding certain failures.

### Manufacturing

Prototyping our design lead us through numerous manufacturing processes, which in many cases were dead-ends. The main cause of inconsistency and frustration was due to using the improper equipment, which in our case was a weak plasma oven that did not provide consistent bonding. We used a plasma oven which did not bond our samples effectively and this caused us to pursue molding with a water-jet aluminum negative and to throw out our efforts in laser-cutting the PDMS samples. Laser-cutting the

PDMS provided very good interior features and changed the surface quality slightly, which is why we thought it did not bond well. However, the same poor bonding occurred with molded samples due to the low quality plasma oven we were using and we cannot prove that the bonding failures were due to the laser cutting. More experimentation should be done with laser cutting the PDMS to prove or disprove its feasibility. Also, a major time-drain in manufacturing was due to punching holes in the PDMS, which limited the diameter of holes being punch to the availability of the same diameter hollow needles. This problem can be addressed by incorporating the holes into a mold or also by pursuing laser-cutting the holes.

**Future Work**

A necessary advancement in this area of research is to bring the technology down to a MEMS level which will simplify discovered problems that occur at the large scale. At the current scale, manufacturing a mold using lithography and a silicon wafer is not necessary or feasible due to the other large components involved in the system; however it would be necessary at a MEMS level and highly tolerance perfect molds could be formed. The whole system could be manufactured at a micro-scale and this would involve incorporating micro-valves and channels, which would replace the need for exterior tubing and exterior valves. With no exterior tubing or valves, the gas leakage problems with our prototype would not occur and it would also reduce large tubing costs, while the smaller valves would require less electrical energy than the current large system.

## CONCLUSION

We have successfully designed and prototyped a pneumatically actuated bubble tactile display which provides necessary research in order to advance the pneumatic tactile actuation technology. Our system design focuses mainly on the pneumatic actuator array (tactile pad) and incorporates standard manufactured components into the assembly of the complete system, which are to be compacted and made more efficient with additional research. In order to design a perceptible and functional tactile pad, we reviewed material on tactile perception, similar tactile devices, manufacturing materials, and relevant technologies which allowed us to pursue areas of limited research and build on current technologies. This lead us to design a system with a 16 bubble actuated tactile pad that has varying bubble diameters from 1.00 - 1.75 mm. The pad is manufactured almost entirely out of polydimethylsiloxane (PDMS), which is used extensively in micro-fluid applications. Each bubble can be individually actuated and operate at pressures around 30 Psi with the aid of 16 3-way solenoid valves and a high-pressure $CO_2$ tank-regulator system. By prototyping our design, we identified a possible manufacturing process for our tactile pad and were able to recommend small design improvements based on the prototype's performance. The prototype also allowed us to conduct some preliminary physical and psychological tests, whose results indicate an experimental free bubble displacement of 30% greater than the theoretical displacement and improved perceptibility associated with bubble diameters of 1.2 mm versus 1.4, 1.6, and 1.8 mm diameter bubbles. With our research and results, the research in pneumatic tactile displays can be steered in an appropriate direction which may one day lead to optimal tactile stimulation and optimal human-to-computer or human-to-human interactions.

## APPENDIX A

### Supplemental Design Drawings

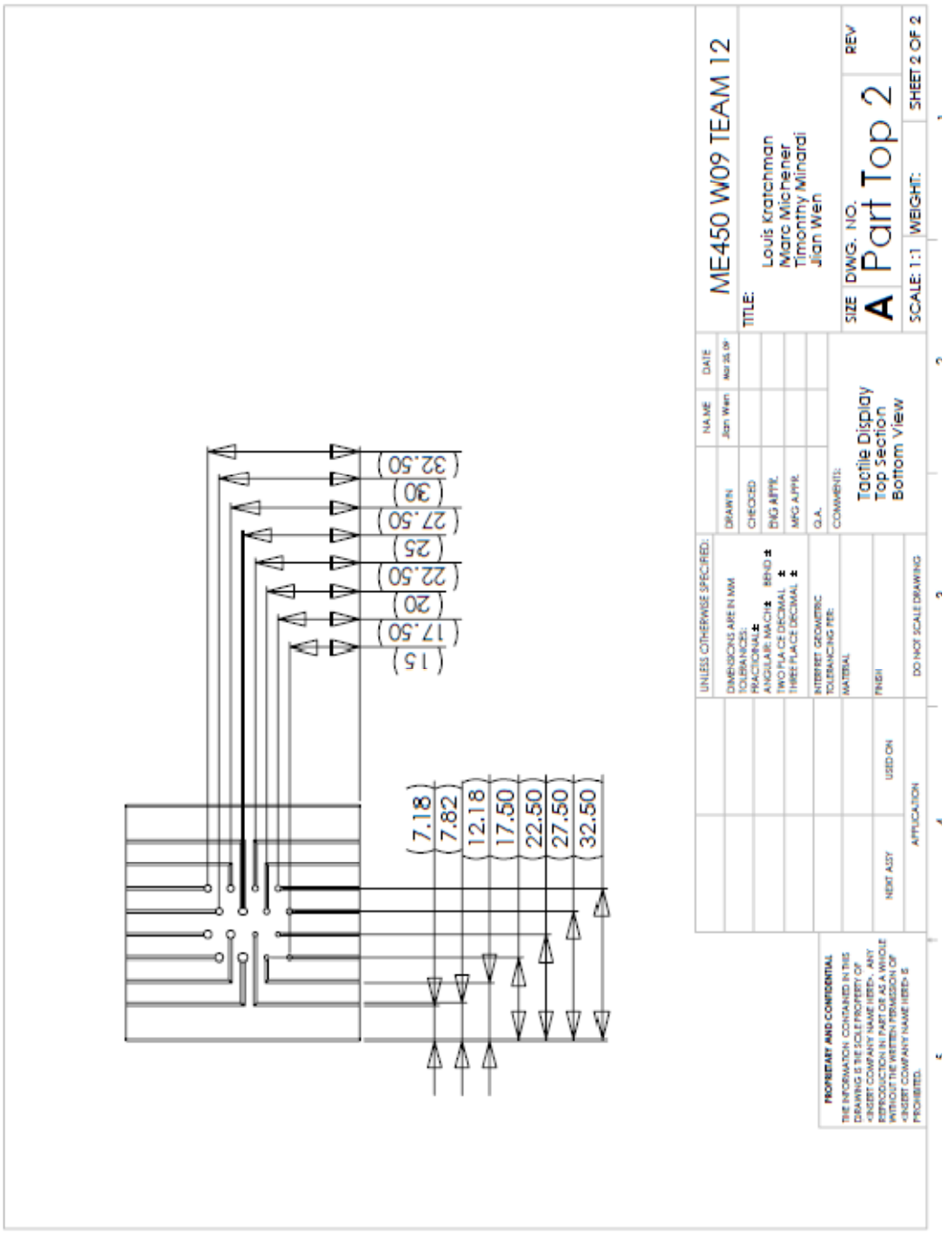


**Figure 40:** Engineering drawing of tactile array assembly

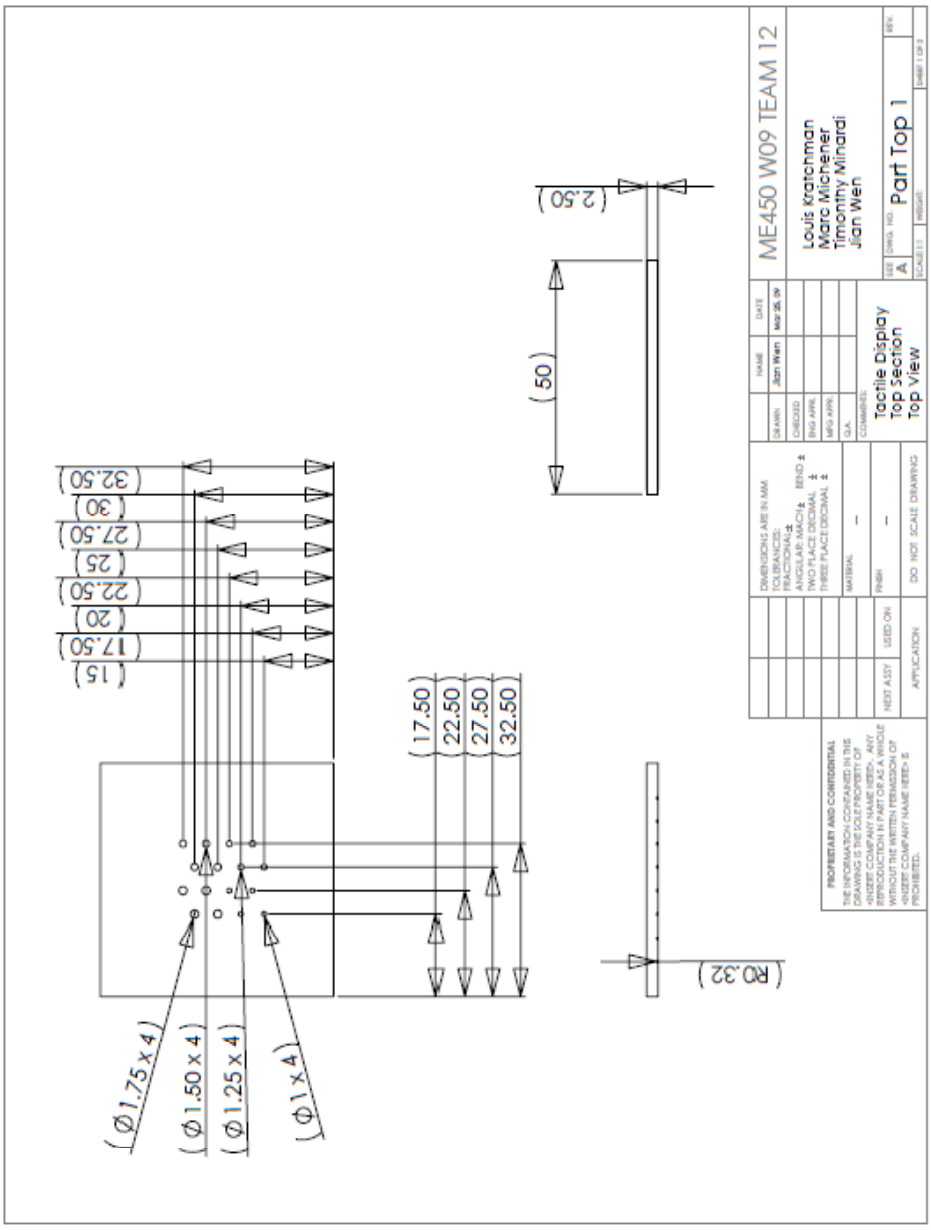


**Figure 41:** Engineering drawing of tactile array assembly

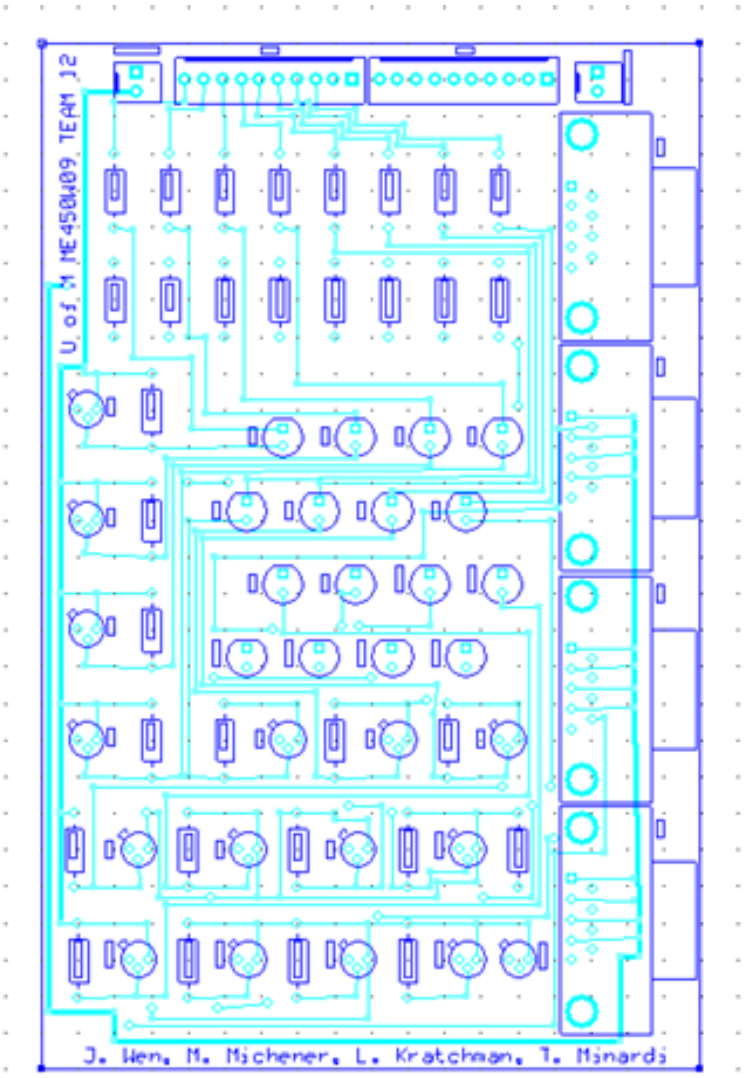


**Figure 42: P**rinted circuit board (top view)

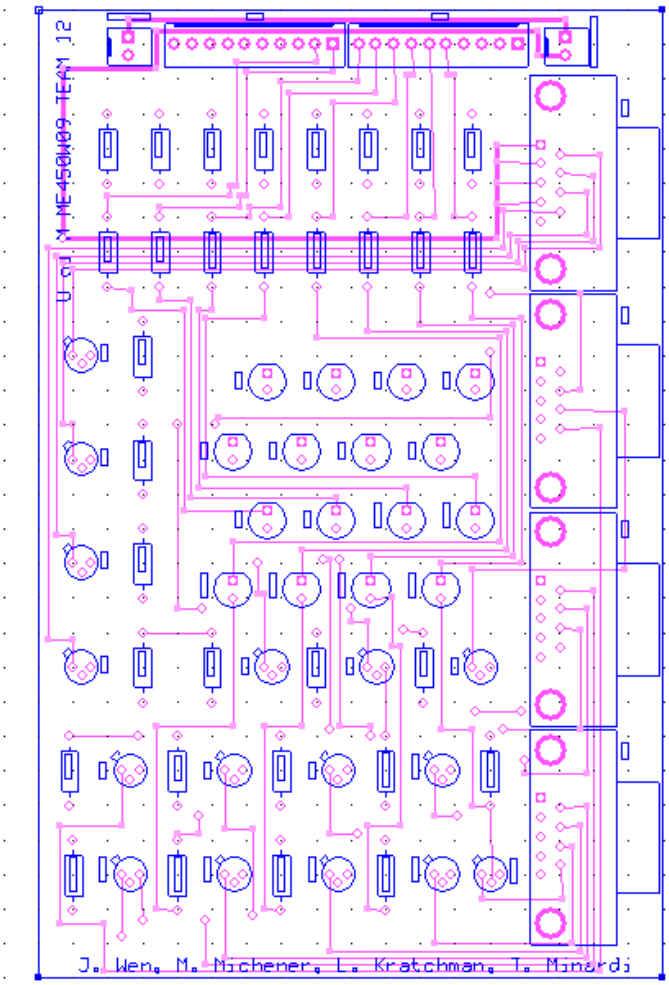


**Figure 43: P**rinted circuit board (bottom view)

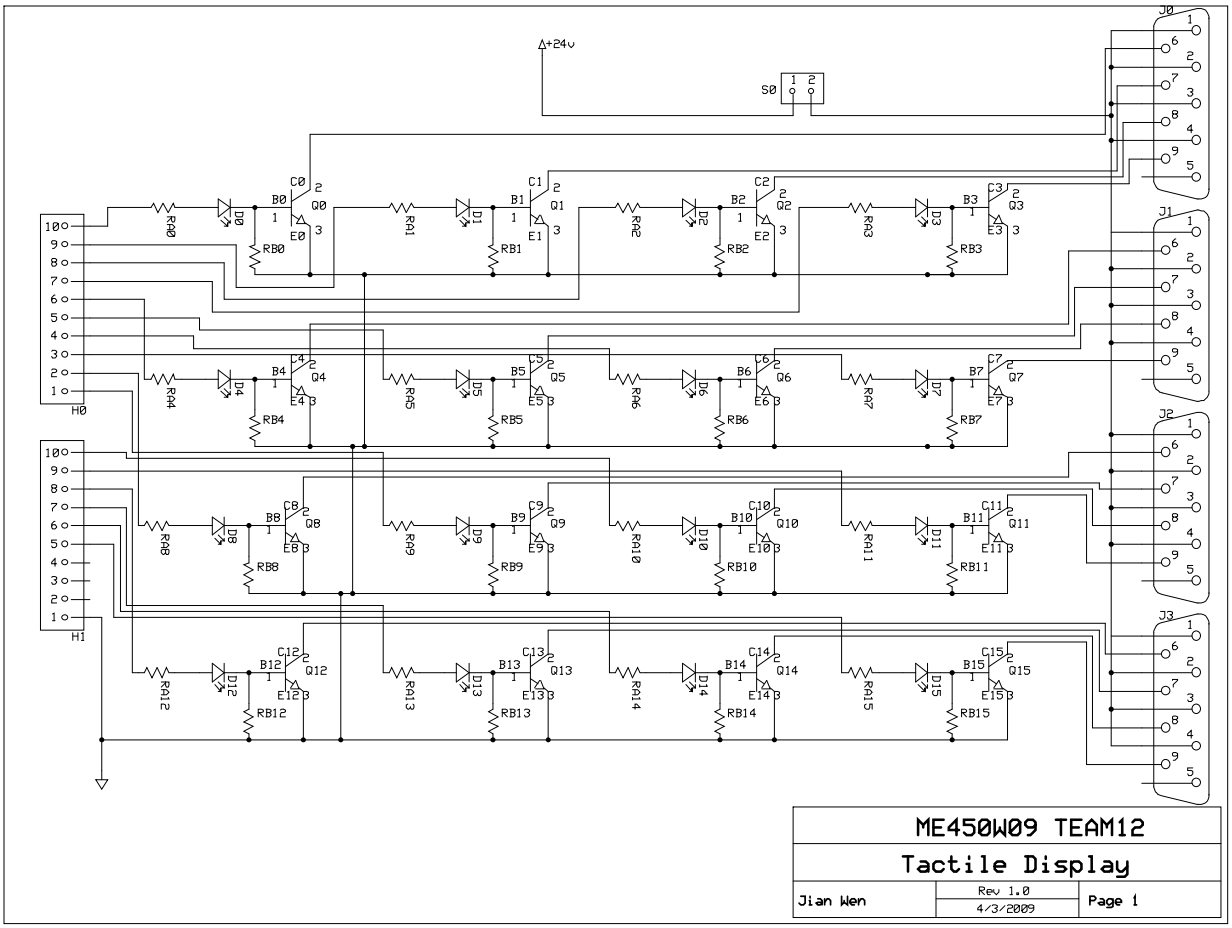


**Figure 44:** Circuit schematic

## APPENDIX B

### Use of CES Software to Aid Material Selection

Our initial candidate materials for the tactor pad and elastomer were selected using CES software. This analysis yielded a large number of candidates, which we further restricted by considering price, machinability, toxicity, and appearance. Figs. 45 and 46 illustrate the wide field of candidate materials, which we will further restrict with upcoming in-depth mechanical analysis of our system.

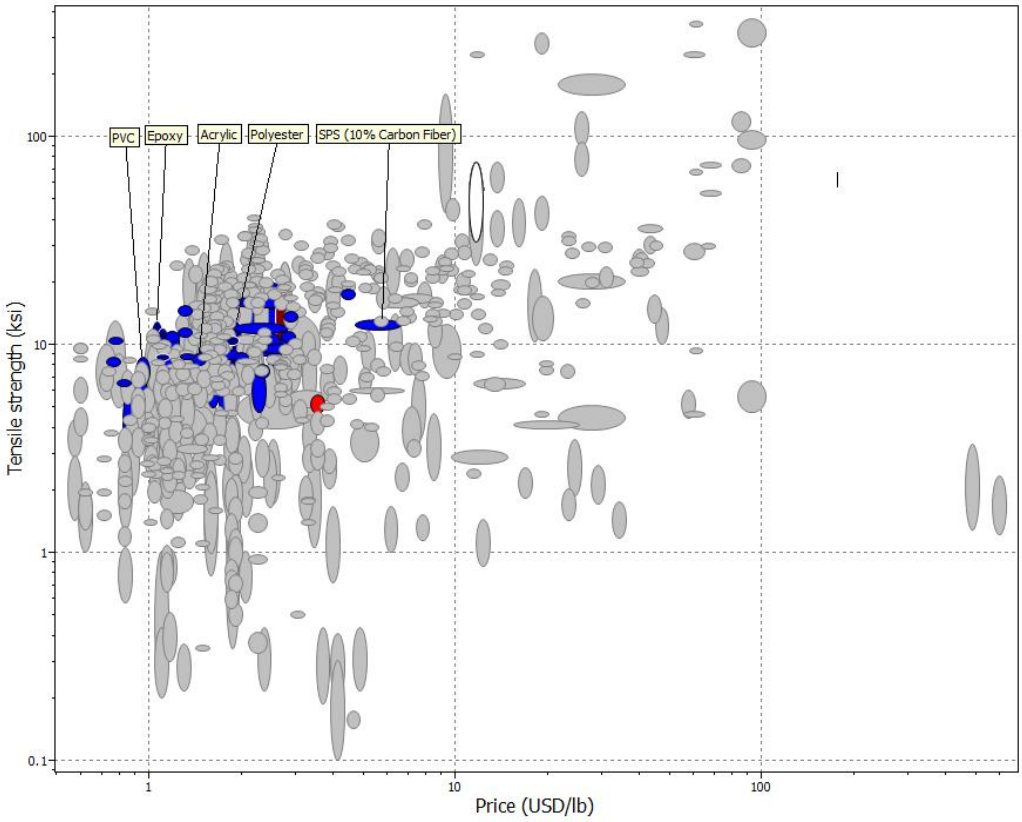


**Figure 45:** CES software material selection for the tactor pad

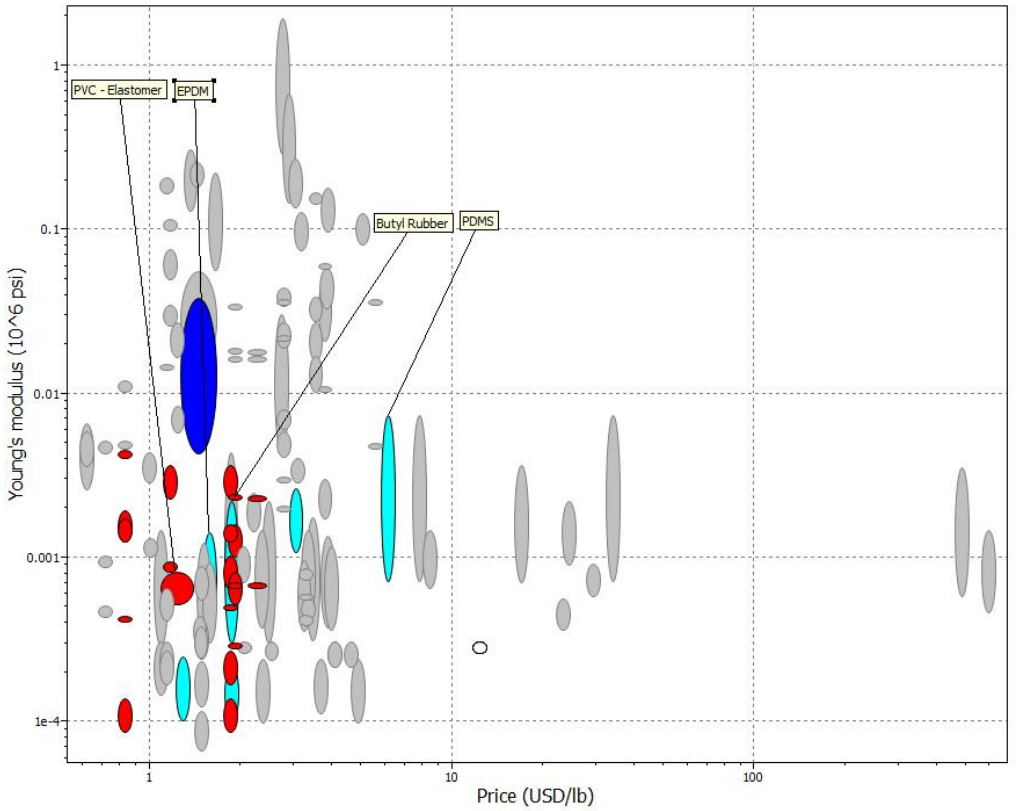


**Figure 46:** CES software material selection for the elastomeric membrane

## APPENDIX C

### Additional Concepts Generated for Lateral Tactors

We entertained variations within five main categories of tactor design, where we struggled with the problems of developing adequate force and displacement in the lateral plane as well as manufacturability. Images conveying the essential concept in each category are shown in Figs. 7-11 on pp. 10-12.

**Pistons**
Most of our concepts in this category used a round piston and considered variations in transmitting the piston's force to the finger above the row of cylinder holes and preventing pressure loss from escaped air. Additional variations included:

- Submerging the cylinder hole entirely below the pad surface, using a mechanical link at the end of the piston to transmit force to the surface (analogous to the connecting rod attached to a piston in an automobile, but using a rigid linkage or compliant mechanism rather than a joint linkage with machined parts). This approach would minimize air leakage.
- Fig. 7 shows a thin, sliding plate for preventing air loss covering the slot which connects the piston to the pad surface. We considered replacing this plate with a loose, flexible, thin boot which would stretch throughout each cycle, preventing air loss without excessive stiffness opposing the motion.
- Replacing the tiny coil spring that returns the piston to its initial position shown in Fig. 7 with a compressible foam, compliant mechanism spring, or double-ended cylinder (with air ports on both end of the cylinder to alternate the direction of motion).

All of the ideas in this category required precise fabrication of tiny components. After experimenting with fabrication of holes and channels, we became skeptical of our ability to manufacture and assemble components at the scale required for this concept within acceptable tolerances. While we considered the piston family of concepts viable at larger scales, we ultimately ruled it out completely due to incompatibility with available manufacturing processes.

**Horizontally Mounted Bubble Rows**
Using horizontal rows of bubbles allowed us to concentrate on amplifying the lateral bubble motion. Fig. 8 on pg. 11 is a simplified depiction of the lever principle used in all iterations of this concept. We considered using a rectangular lever arm (with width approximately equal to the bubble) embedded with its (horizontal) fulcrum in a flexible membrane suspended over the rows of bubbles. We also considered using a vertical fulcrum axis (attached to a support via a compliant hinge), with an L-shaped lever rotating in the plane. Both of these approaches require a substantial amount of space for the levers to sweep out their trajectories. The horizontal-axis fulcrums would increase the thickness of the device, while the vertical-axis fulcrums would pose spacing difficulties.

**Bourdon Tubes**
Our Bourdon Tube concepts, described on pg. 11, all assumed the tubes would be actuated in the plane, and involved variations on the geometry of the tubes themselves and the processes for manufacturing them. We discussed methods for molding the bubbles both in place (on the tactor pad) and as separate objects to be bonded to underlying tubing on the tactor pad.

To mold the tubes in place, we considered using layers of low melting point sacrifical wax to separate the tubes when molded from the underlying pad material. The tubes would be formed in two pieces, a

channel overlayed with a membrane to enclose the tube. After enclosing the tubes, the wax piece could be heated to drain the wax through the air tubes.

Alternatively, we considered crescent-shaped molds out of wax, and coating the molds with elastomer by dipping them in a bucket of fluid elastomer. After solidifying the elastomer, the tubes could be heated to drain the wax and then bonded to flow holes on the tactor pad.

Due to the size of our device, we were concerned that the sacrificial wax would be difficult to shape precisely and would be even more difficult to drain completely from the device, leaving residual air flow restrictions. Moreover, we became skeptical that tubes made from a flexible material would be able to generate sufficient force without collapsing. We considered geometries with stiffening ribs to prevent collapse, but ultimately concluded that the pick intended for the end of the tube would easily torque the end of the tube and the force would be lost in this twisting.

**Tilters**
We were initially impressed with the simplicity of the tilter concept, described on pg. 12. We considered the following possibilities:

- Using two bubbles with a cross-bar affixed to them. This approach would be simplest to manufacture, but would require a very long vertical piece and would require twice as many bubbles as tactors.
- Using a single bubble with a tilting surface, and grounding the opposite end of the tilting surface to the tactor pad. The end attached to the tactor pad would require a flexible, compliant hinge to allow rotation.
- Using the 'pneumatic artificial muscle' concept: protruding enclosed chambers which when pressurized inflate in their midsections and decrease in height. Using this concept would allow much more displacement than elastomer bubbles, and could be manufactured by dipping a negative mold of protruding cylinder shapes into liquid elastomer.

**Hairs**
Variations on the "hair" concept discussed on pg. 12 involved the stiffness of the hair material, the thickness of the hairs, and the spacing of the hairs. At one extreme we considered covering the entire membrane with a dense layer of animal-like fur, but concluded it would be very difficult to localize the source of the actuation due to the bending and spreading of adjacent hairs. At the opposite extreme, we consider using rigid wires, though we realized that securely embedding the base of such objects in a flexible membrane would be nearly impossible. Our best candidate in this category was densely packed thick elastomeric stalks.

**APENDIX D**

**Survey of Tactile Actuation Methods**

Most approaches to tactile displays feature a single dominant transduction or energy transmission technique, and in the following discussion we consider notable achievements in each actuation category. In Table 5 below, we present a side-by-side comparison of key numerical parameters, though we caution that the figures should not be used for ranking purposes. The overriding consideration is effectiveness at transmitting data through the tactile perceptual system, a figure which cannot be readily quantified for comparative purposes. While some designers conducted rudimentary psychophysical experiments with human subjects, no such results are available for many others, and we must turn to our basic scientific understanding of the sense of touch to discern the most promising approaches.

| Tactile Display | Tactor Diameter | Tactor Spacing | Bandwidth | Tactor Array | Pad Thickness | Displacement or Force |
|---|---|---|---|---|---|---|
| Pneumatic Bubbles [6] | 3.0 mm | 1.5 mm (E) | 8-10 Hz | 3 x 2 | 0.4 cm | n/a |
| Air Jets [7] | 1.5 mm | 2.4- 3.2mm (C) | 0-50 Hz | 5 x 5 | n/a | n/a |
| Pneumatic Pins [8] | 1.02 mm | 2.5 mm | 0- 5Hz | 5 x 5 | n/a | 0.7 mm |
| Ultrasonics [19] | 1.0 mm | n/a | 20 Hz–1 kHz | 6x6 | n/a | 0.9 mm |
| Thermal Phase Change [21] | 3 mm (square) | 3 mm (C) | n/a | 3 x 3 | 1 mm | 48 μm |
| ER Fluid [22] | 11 mm (square) | 13 mm (C) | Static | 5x5 | 2.5mm of fluid | 2-3 N |
| MR Fluid [23] | n/a | n/a | Static | 1x1 | n/a | 2-3 N |
| Dielectric EAP [24] | 2 mm | 3 mm (C) | 0-150 Hz | 4x5 | 0.255 mm | 0.9-0.7 mm |
| Ionic EAP [25 ] | 10 mm | n/a | 1 Hz | 3x3 | n/a | 0.45 mm |
| Piezo w/Membrane*[26] | n/a | n/a | 0-1000 Hz | 12x12 mm | n/a | n/a |
| Piezo Bimorph*[27 ] | 1 mm (length) | 1 mm (C) | 0-700 Hz | 10x10 | n/a | 25μm |
| TULA [28] | n/a | 1.5 mm (C) | 0-20 Hz | 4x8 | n/a | n/a |
| Electromagnetic [29] | 1.6 mm | 2 mm (C) | 0-300 Hz | 4x4 | n/a | 5 mN 2-6 mm |
| SMA [30] | 1.5 mm | 2.6 mm (C) | 1.5 Hz | 8x8 | 8 cm | 320 mN 1 mm |
| Microhydraulic [32] | 1.57 mm | 2 mm (C) | 5.5 Hz | 1x5 | n/a | 2 mm |

~ * indicates lateral movement of tactor
~(E) indicates edge-to-edge spacing and (C) indicates center-to-center

**Table 5:** List of key parameters for competitor tactile displays

**Ultrasonic**
Focused sound waves can produce perceptible skin displacements to form a tactile display. One group [19],[20] used a phased ultrasonic array (an arrangement of piezoelectric transducers which allows precise

focus of ultrasonic wavefronts) to direct acoustic energy through a gel or water medium to a foam rubber sheet (Figure 50), upon which fingers were placed. Rather than using a discrete number of tactors, the array rapidly scans the target area. A 1 $cm^2$ grid divided into 1 $mm^2$ targets (which may effectively be considered tactors) can be scanned in 1 ms, though the beam location can in theory be varied continuously. Peak tactile sensitivity was observed when modulating the ultrasonic carrier waves with square waves at 30 Hz and 200-250 Hz. The device generated a peak force of 1.9 $gf/cm^2$. The precise beam position control, and rapid refresh rates of the technology seem promising, though little psychophysical testing has been conducted, and no point discrimination test results are available.

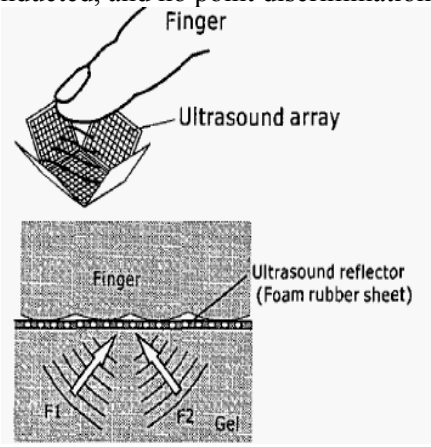


**Figure 50:** Ultrasonic Tactile Array [19]

**Thermally-Activated Phase Change**

When an enclosed fluid is vaporized by heating, the large increase in volume can be used to displace skin in a tactile display. One novel approach [21] incorporated the phase change principal into a tiny (15x15x1 mm) microfabricated array of nine tactors. Each tactor (Figure 51) consisted of an electric heater, a low boiling point liquid, and a PDMS membrane with a needle attached to precisely stimulate the skin. The heater creates a vapor bubble, displacing the membrane. The device achieved a maximum needle displacement 48 μm in testing, but time delays on the order of 1ms were needed to obtain substantial displacements, and no psychophysical testing was performed. We take this device into consideration as a demonstration of the miniaturization possible with MEMS fabrication techniques and for its use of a needle to focus the energy transmitted by an inflatable bubble.

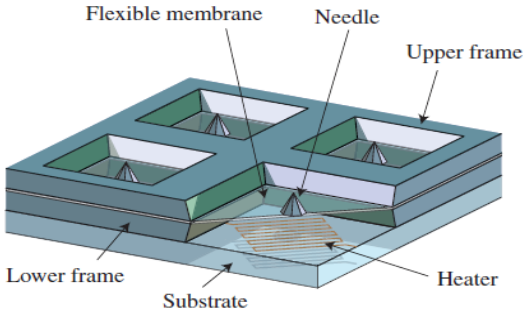


**Figure 51**: Thermally-Activated Phase Change Display [21]

**Electrorheological (ER) and magnetorheological (MR) fluids**

Electrorheological and magnetorheological fluids are a special type of dielectric fluids whose rheological properties change when exposed to an external electric or magnetic field. This is due to the dielectric fluid being laced with small particles which line up with an externally applied field. This causes the fluid's viscosity, and therefore its yield strength, to increase [22]. We have reviewed two cases in which the researchers used this technology to create a tactile array. The first case used an ER fluid to create a 5x5

array (Figure 52), which possessed tactors that had an area of 11 $mm^2$ and were able to produce resistive forces normal to the fluid surface. The array was only tested under static conditions and the tactors were able to produce around 2-3 N resistive forces, which were not uniform among the tactors [22]. In the second case (Figure 53), a MR fluid was used to create only a large 1x1 array which produced static resistive forces around 2-3 N as well [23]. In both cases it they had created largely sized arrays and did not provide any information about the dynamic performance of the tactors. The actuated tactor did not seem to rise up above the fluid, but to resist force when the rest of the fluid was displaced as something rolled along the surface. Also it seemed as though fluids acted inconsistently with the applied fields which lowers the total control of the systems.

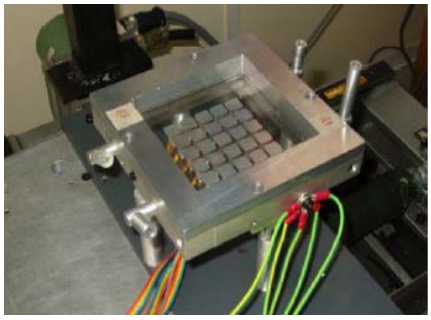

**Figure 52**: ER Fluid Array [22]

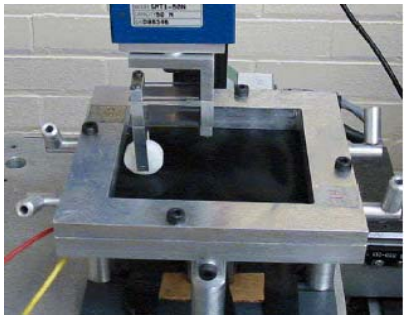

**Figure 53**: MR Fluid Array [23]

**Electro-Active Polymers (EAP)**

One of the most promising actuators was electro-active polymers and we reviewed two types, dielectric and ionic. Both types consist of a polymer sandwiched between two capacitive plates, but they cause motion in totally different ways. The dielectric type utilizes a strong electric force to cause the polymer to shrink vertically and elongate laterally, causing motion [24]. This was utilized in one project where a 4x5 array of dielectric EAP actuated tactors was created and it produced normal indentations (Figure 54). The tactile cells were 2 mm in diameter and the unit was only about 0.25 mm thick. This array was able to cause 0.9 mm displacements at static conditions and around 0.7 mm displacements at 150 Hz [24]. The other type of EAP (ionic) causes motion by ionic movement within the polymer when an electric field is applied. This movement causes a density imbalance which actuates the material. This was used in creating a 3x3 array (Figure 55) that produced normal indentations. The array contained 10 mm diameter tactile cells and could make 0.45 mm displacements at a frequency of 1 Hz [25]. The dielectric EAP group was one of the few current researchers able to create a functioning wearable tactile prototype; however, it did required operating voltages in the kVolt range. The ionic style EAP was good in the sense that it required minimal voltages (~1 V), but it did not possess a large enough displacement or bandwidth to compete with the dielectric EAP.

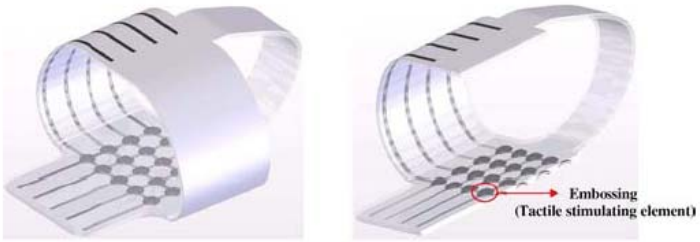


**Figure 54:** Dielectric EAP Actuated Array [24]

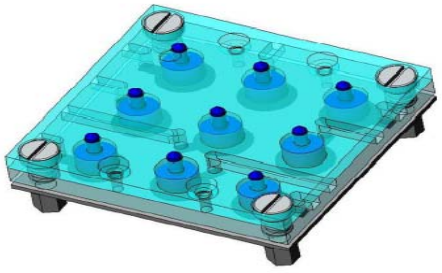

**Figure 55:** Ionic EAP Actuated Array [25]

**Piezoelectric**

Piezoelectric ceramics are widely used in tactile displays and they provide actuation because their crystalline structure changes when exposed to an electric field, which causes them to strain [18]. One reviewed prototype using piezoelectric actuators consisted of a 64 actuator array that actuated a 112 tactor membrane (Figure 56). The membrane was 12x12 mm in dimension and could operate at frequencies up to 1000 Hz. An interesting feature of this prototype was that the membrane converted vertical actuation into lateral movement with the membrane [26]. A different prototype utilized piezoelectric bimorphs to create a 10x10 laterally-actuating tactile array (Figure 57). The actuators were spaced 1 mm center-to-center and had a tip displacement of 25 μm at frequencies up to 700 Hz [27]. The final piezoelectric prototype reviewed contained a 4x8 array (Figure 58) which was actuated with the aid of 16 Tiny Ultrasonic Linear Actuators (TULA) and produced normal indentations. The TULAs were composed of piezoelectric materials that operated at ultrasonic frequencies when the motor itself could only move at a rate of 20 mm/sec. This array had tactor spacing of 1.5 mm center-to-center and could operate at frequencies up to 20 Hz [28]. In the first two piezoelectric arrays mentioned, there was a small array but they seemed to be accompanied by large actuator bases and control circuits. The array with piezoelectric bimorphs had limited displacement (25 μm), but the actuators may have been stacked closed enough to allow for several small actuators to act as one and this showed potential. The array containing the TULAs operated a lower than optimal frequencies to stimulate the skin and the TULAs were a little large so they had to link two tactor to each motor because of spacing issues.

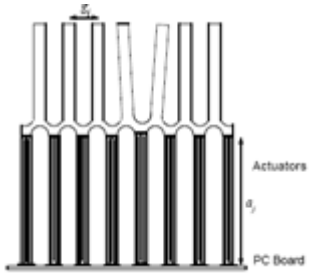


**Figure 56:** Membrane Array [26]

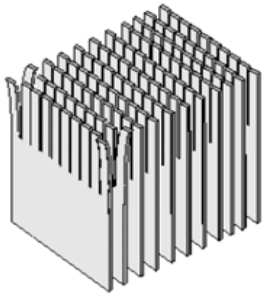

**Figure 57:** Bimorph Array [27]

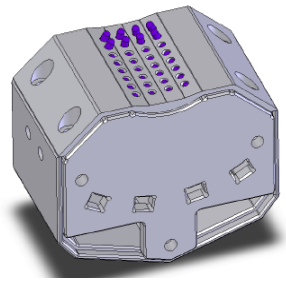

**Figure 58:** TULA Array [28]

**Electromagnetic**

The topic of electromagnet covers a wide range of different actuating devices, such as electric motors, solenoids, voice coils, relays, etc. The general concept of how these devices operate is by passing an electric current through a conducting material to generate electromagnetic forces [18]. These devices then convert the electromagnetic forces into actuating forces. These devices tend to be relatively large compare to other actuating devices. The coil within these devices is the main reason prevents them from reaching smaller size because fabrication of small-scale coils is difficult and because the relative movement is always perpendicular to the coil. This makes it difficult to incorporate EM actuator in planar application. The Joint European Laboratory LEMAC attempted to create a small electromagnetic actuation mechanism using MEMS technology. They modeled an array of 4x4 cantilevers actuated by small magnets and coils (Figure 59). The experiment modeling result indicates a low efficiency of this device in terms of electrical-mechanical energy conversion. It required a current of 800 mA to generate forces of 5 mN [29]. In addition, the prototype would also be cumbersome even with the use of MEMS technology.

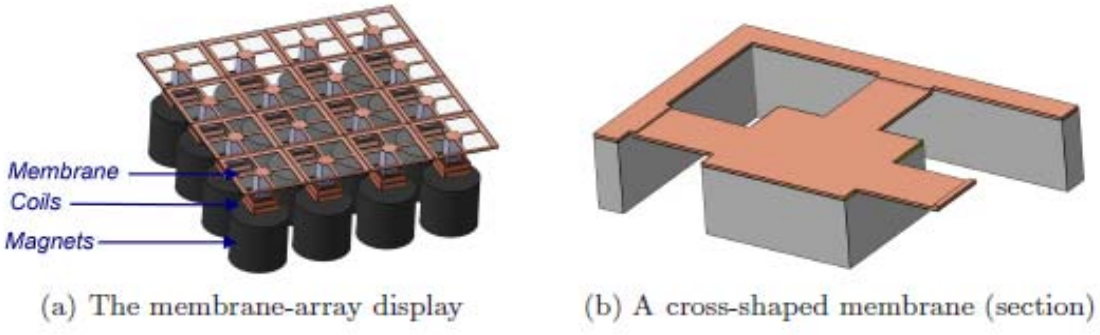


**Figure 59:** Electromagnetic Actuation Base Tactile Display [29]

**Shape Memory Alloy**

The principles behind Shape memory alloy (SMA) are that it consists of a type of material that plastically deforms at temperatures below a critical point, and returning to its original configuration when heated beyond that specific temperature. Due to its unique properties, SMA has been commonly used as an actuation mechanism for small motion. A tactile display using SMA actuators has been developed and evaluated by the Robotics Laboratory of Paris (LRP). The tactile display developed by this group is intended to provide blind subject access to visual information by means of touch simulation. The device contains an array of 8x8 tactile pins which are actuated individually by SMA springs (Figure 60). Using this actuating method, this device is able to achieve 1 mm of displacement, forces of 320 mN, and up to 1.5 Hertz bandwidth [30]. In terms of portability, this device is only 200 gram in weight and a dimension of 8x8 cm, which is a fairly portable. However, there is the unavoidable disadvantage of temperature dependence, which affects possible operating environments and energy usage.

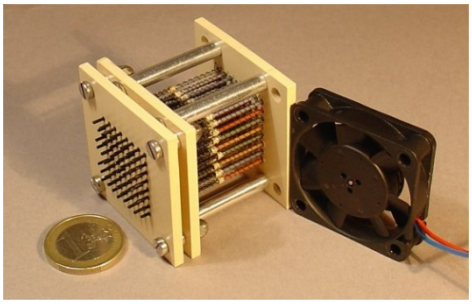

**Figure 60:** Tactile Display Based on SMA [30]

**Electrostatic**

The concept of electrostatic is to use electrostatic charge from a build up or deficit of electrons in a material, which can exert an attractive force on oppositely charge object, or a repulsive charge on similarly charged object, then make use of the electrostatic forces to generate motion. One disadvantage of this type of devices is high voltage requirements. In order to generate enough charges for actuating purpose, the operating voltages often exceed 100V. A research group from Institute of Electromechanical Design in Darmstadt University of Germany has developed electrostatic tactile display with elastic dielectric. The idea is to take advantage of the elasticity of the polymeric dielectric to generate displacement (Figure 61). By applying voltage onto the top and bottom conducting films, electrostatic pressure builds up on both ends of the elastic dielectric, and then a normal displacement then could be generated by deforming the dielectric with enough electrostatic pressure [31]. However, the displacement

on a single film is extremely small mainly because of their 10 um thickness. In order to generate a noticeable displacement, several layers are required, which that pose a challenge in terms of fabricating these devices.

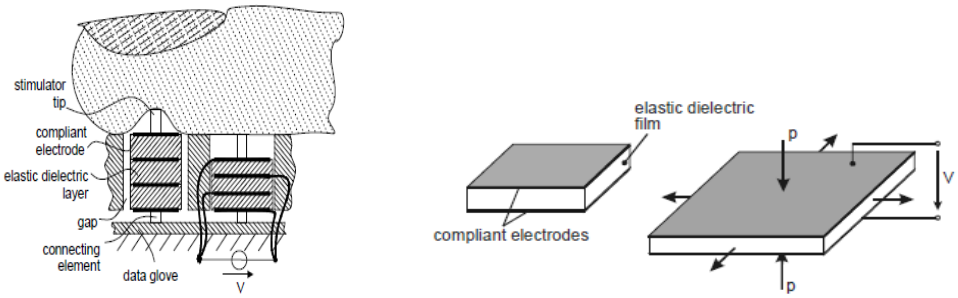


**Figure 61:** Electrastatic Actuation Based on Elastic Dielectric [31]

**Microhydraulic**

Microhydraulic actuation is implements a hydraulic system on a much smaller scale. However, due to the scale, these devices could only operate at a low bandwidth around 10 Hertz or less. The fluid would also heat up due to the friction created between the fluid and the tubing surface at high frequency and this would impact operation. The concept of implementing microhydraulic system onto tactile display devices has been proven by a research group from the Katholieke University. This group has developed a tactile device using the microhydraulic system. The device is powered by servomotors which attach to the microhydraulic system to actuates tactors (Figure 62). Experimental results indicated that the device operates at fairly low frequency of 5.5 Hz [32]. Aside from the low frequency disadvantage, the device has fairly good performance in terms of force output and displacement.

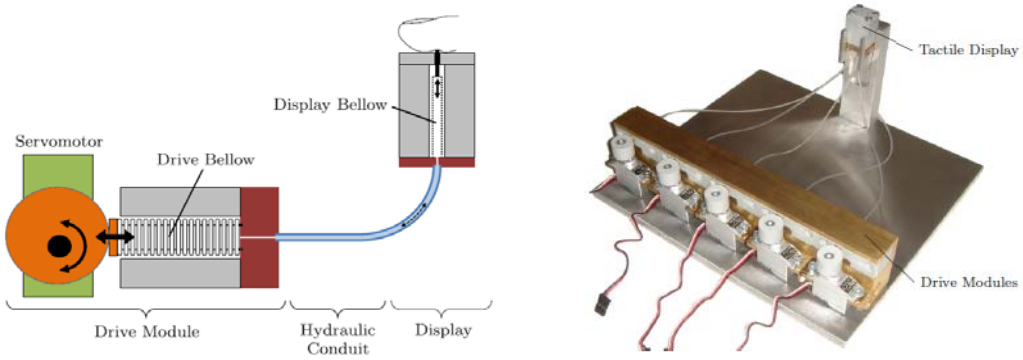


**Figure 62:** Tactile Display Based on Microhydraulic [32]

**Electrohydrodynamic**

Electrohydrodynamic (EHD) actuation (Fig 63) is possible by varying strong electric fields around a dielectric fluid to create fluid flow or pressure [18]. There is no current tactile display that utilizes this technology even thought it has simple electrical to mechanical energy conversion properties. One group at the University of Dayton has come up with a pump actuation concept (Figure 64) that they believe could produce relatively high pressures [33]. This concept could possibly be incorporated into a tactile display and is worth consideration.

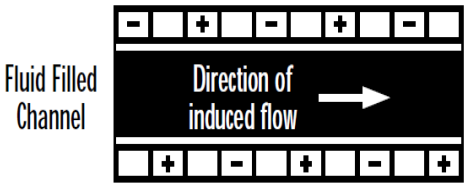


**Figure 63:** EHD Principle [18]

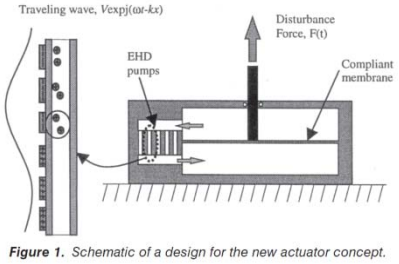


***Figure 1.*** *Schematic of a design for the new actuator concept.*

**Figure 64:** EHD Actuation Concept [33]

## APPENDIX E

## Complete Bill of Materials:

| Component | Catalog/model number | dimensions (mm)/Discription | Website | Pkg Quantity | Puchase Quantity | Price | total |
|---|---|---|---|---|---|---|---|
| Borrowed CO2 Tank | BF C5 | Diameter =140mm; Height= 454mm; Gas Quantity = 2.26 kg; Typical Operating Pressure = 1240 kPa (1800 Psi); | beveragefactory.com | | | 0 | 0 |
| Borrowed CO2 Regulator | BF 742BF | Max inlet Pressure= 1378 kPa (2000 Psi); Max outlet Pressure =413 kPa (60 Psi) | beveragefactory.com | | | 0 | 0 |
| Small polyethylene Tubing | 14-170-11B | ID – 0.581mm; OD –0.965mm | fishersci.com | 3 m (10 ft) | 2 | 27.58 | 55.16 |
| Sylgard 184 Silicone Elastomer (PDMS) | | | ellsworth.com/ | 0.5 kg (1.1 lb) | 1 | 73 | 73 |
| Standard Solenoid Valve | ET-3M-24 | 3 way,NC, 24V, 5-10 ms response | ebay.com | 47 Valves with Manifolds | 1 | 78 | 78 |
| Needle Fittings | 75165A684 | ID= 0.432mm; OD= 0.635mm; length = 12.7mm | mcmaster.com | 50 | 1 | 13.97 | 13.97 |
| Reusable Needle for Manufacturing | 6710A21 | ID=1.60mm; OD= 2.11mm; length=50.8 mm | mcmaster.com | 1 | 1 | 3.85 | 3.85 |
| Reusable Needle for Manufacturing | 6710A23 | ID=1.20mm; OD= 1.65mm; length=50.8 mm | mcmaster.com | 1 | 1 | 3.75 | 3.75 |
| Reusable Needle for Manufacturing | 6710A26 | ID=0.69mm; OD= 1.07mm; length=50.8 mm | mcmaster.com | 1 | 1 | 3.6 | 3.6 |
| Reusable Needle for Manufacturing | 6710A28 | ID=0.51mm; OD= 0.81mm; length=50.8 mm | mcmaster.com | 1 | 1 | 3.49 | 3.49 |
| Reusable Needle for Manufacturing | 6710A48 | ID=0.25mm; OD= 0.46mm; length= 101.6 mm | mcmaster.com | 1 | 2 | 3.76 | 7.52 |
| Reusable Needle for Manufacturing | 6710A19 | ID=1.80mm; OD= 2.41mm; length=50.8 mm | mcmaster.com | 1 | 1 | 3.9 | 3.9 |
| Reusable Needle for Manufacturing | 6710A18 | ID=2.16mm; OD= 2.77mm; length=50.8 mm | mcmaster.com | 1 | 1 | 3.96 | 3.96 |
| Reusable Needle for Manufacturing | 6710A22 | ID=1.37mm; OD= 1.83mm; length=50.8 mm | mcmaster.com | 1 | 1 | 3.8 | 3.8 |
| Reusable Needle for Manufacturing | 6710A24 | ID=1.07mm; OD= 1.47mm; length=50.8 mm | mcmaster.com | 1 | 1 | 3.7 | 3.7 |
| Reusable Needle for Manufacturing | 6710A25 | ID=1.84mm; OD=1.77mm; length=50.8 mm | mcmaster.com | 1 | 1 | 3.65 | 3.65 |
| Ribon Tubing | 50555K71 | 1/16" ID | mcmaster.com | 1 ft | 10 | 0.88 | 8.8 |
| L Bracket | 1556A16 | 3.5" Length Sides | mcmaster.com | 1 | 2 | 1.42 | 2.84 |
| Terminal Connectors | 7243K112 | Dbl Crimp 22-18 AWG 0.187" Wide | mcmaster.com | 25 | 3 | 7.16 | 21.48 |
| Luer Needle Connector | 51525K121 | Male x barb for 1/16" tubing | mcmaster.com | 10 | 3 | 3.69 | 11.07 |
| Aluminum Sheet | 89015K12 | 305 x 305 x 1.02 mm ; Alloy 6061 | mcmaster.com | 1 | 1 | 11.21 | 11.21 |
| Printed Circuit Board | XAUD-4B5-M | Custom Circuit Board | expressPCB.com | 1 | 1 | 55 | 55 |
| D-Sub Connectors | 747840-4 | DB-9, Male PC Mount | surplussales.com | 1 | 4 | 4.5 | 18 |
| D-Sub Connector Housing | 276-1539 | Single unit package | Radioshack | 2 | 4 | 3.75 | 15 |
| Basic Stamp Microcontroller | 276-625 | Microcontroller Kit | Radioshack | 1 | 1 | 55 | 55 |
| Project Enclosure | 270-1806 | 6 inch x 4 inch x 2 inch | Radioshack | 1 | 2 | 5 | 10 |
| Assorted LED Package | 276-1622 | Package of 20 assorted LED | Radioshack | 20 | 5 | 3 | 15 |
| LED Holders | 276-080 | Package of 2 LED holders | Radioshack | 2 | 8 | 2 | 16 |
| Acrylic Base | | 12" X 24" x 0.25" clear acrylic sheet | Stadium Hardware | 1 | 1 | 14 | 14 |
| Rubber Feet for Acrylic Base | | Clear rubber feet | Stadium Hardware | 15 | 1 | 3.79 | 3.79 |
| CO2 Refill | | | airgas (State Street) | | 5 lbs | 20.14 | 20.14 |
| | | | | | Grand Total | $ | 618.7 |

## APPENDIX F

### Fluidic Logic

Fluidic logic has been investigated as a replacement of transistors for performing logical operations during the 1950s, and the research has largely been limited by the manufacturing technology at the time, so no significant progress was made during that period. Until recent years, the advancement of MEMS technology has enable researchers to fabricate and manipulate microfluidic devices in a way that have not been possible before. Most research has been focused on medical applications in this technology. A great example would be lab-in-a-chip, where the samples are mostly fluidic substances. As the technology advances, these devices are not only responsible for obtaining data but to analyze it as well. In order to analyze the data, computational algorithms are being developed and incorporated into the devices which require the concept of fluidic logic. Several groups of researchers have successfully developed microfluidic devices that implement simple logics, such as OR, AND, NOT, etc.

As the number of tactors increases, the tubing of the entire system could be problematic and could cause low efficiency as well. Therefore, we investigated this technology of fluidic logic to seek improvements in terms of simplifying the structure of our device and also minimizing the power dissipation by implementing logic through fluid instead of electricity.

**Fluidic Logic Literature Review:** Microfluidic device for logic has the same fundamental principal as transistors. It starts out as a switch, and the complexity increases with functionality. The basic operation of a fluidic logic unit is a switch for a flow as shown in Figure 65. The flow is controlled by the pressure in the cavity below and the membrane acts as a valve for opening and closing. As the cavity gets pressurized by the control valve, the membrane would be pushed against the blocking cap and no flow is allowed. As the cavity gets vacuumed, the membrane would be pulled away from the blocking cap and flow is allowed.

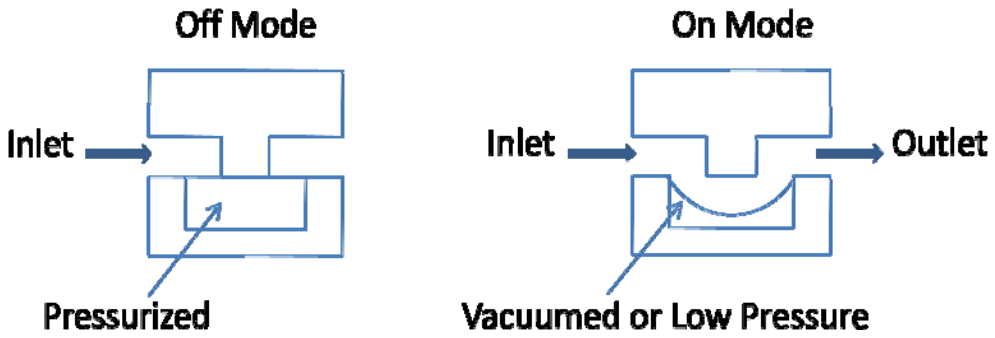


**Figure 65**: On/Off Switching Implementation

This is a simple on/off switch for controlling the flow. Several on/off switching methods have been developed by different research groups. However, PDMS membrane was used as open/close mechanism in all these methods we came across so far. The unique properties of PDMS material and its developed manufacturing techniques have made it the ideal candidate for these types of application.

By manipulating this switching operation, logic functions of NOT, OR, AND, etc could be implemented using fluidic microdevices. Examples of NOT and OR logic functions are illustrated as followed:

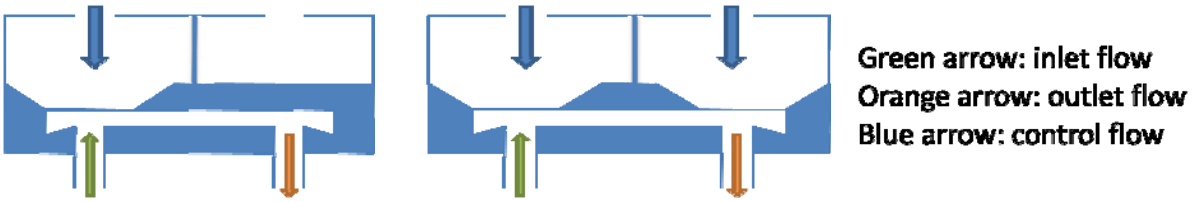


**Figure 66**: NOT Logic (Left), OR Logic (Right)

When control flow is inactive (input=0), the flow is allowed (output =1); when control flow is active (input=1), the flow is blocked by the expanding membrane (output=0). This satisfies the NOT logic operation. When either or both of the control flow is active (input A or/and B = 1), the flow is blocked by either or both membrane; only when both of the control flow is inactive (input A and B = 0), the flow is allowed. This satisfies the OR logic operation. Any type of logic functions could be generated from the simple on/off switching operation.

With the proper use of the logic functions, we could use less number of tubing and still achieve the same functionality. Base on our calculation for a 4 x 4 array, we would only need five ingoing tubes and valves for actuating the 16 tactors individually. This simplification is traded with a complicated manufacturing process to craft out the necessary geometry in each layer in order for the logic to be implemented. An exploded view of NOT logic function is provided (Fig. 67) to show the complexity of manufacturing procedures. Due to the microscopic nature of these devices, fabricating these layers still remain challenging to us in terms of the fabrication techniques that are available for us.

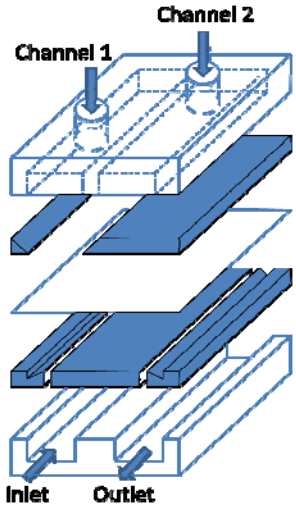


**Figure 67:** Exploded View of NOT Logic

**Issues related to the implementation of fluidic logic**

Even though the fluidic logic offers great advantages in terms of simplifying tubing complexity and increase efficiency, it has limitations as well. One of the limiting factor is the pressure within the system has to be closely monitored to ensure proper implementation of the logic functions. A research group from Feng Chia University, Taiwan has conducted experiments on the NOT logic as shown in Figure 66. This group has determined that for an inlet flow of 27.58 kPa with a flow rate of 0.375 cm/s, the control flow has to be between 55.16 kPa and 82.74 kPa for proper logic implementation [34]. For control flow less than 55.16 kPa, the membrane cannot seal the inlet flow completely. For control flow higher than

82.74 kPa, plastic deformation occurred and seriously affected the switching response. The operating pressure range is a concern for us because we want to generate a minimal lateral displacement that could perceive by human skin, which is 0.9 mm. In order to achieve that, the actuating bubble would require substantially higher pressure (at least 100 kPa) than the test results, which lead us to re-evaluate the feasibility of implementing fluidic logic without mass modifications to the entire structure.

Research groups have conducted experiments to test the performance of their fluidic logic devices. The response time of these devices is ranging from hundreds of millisecond to couple of seconds. For the purpose of our device, response time of fluidic logic is a concern for us. The group from Taiwan has timed the propagation delay for a simple NOT logic to be 700 ms ($t_{pHL}$) and 320 ms ($t_{pLH}$) of a 5 valve device using microfluidic logic as shown in Figure 67. Based on their results, a minimal pneumatic pulse of 80 ms is required for a correct latching operation [35]. A cycle time of almost 2 seconds is measured for a sixteen multiplexed latching valves.

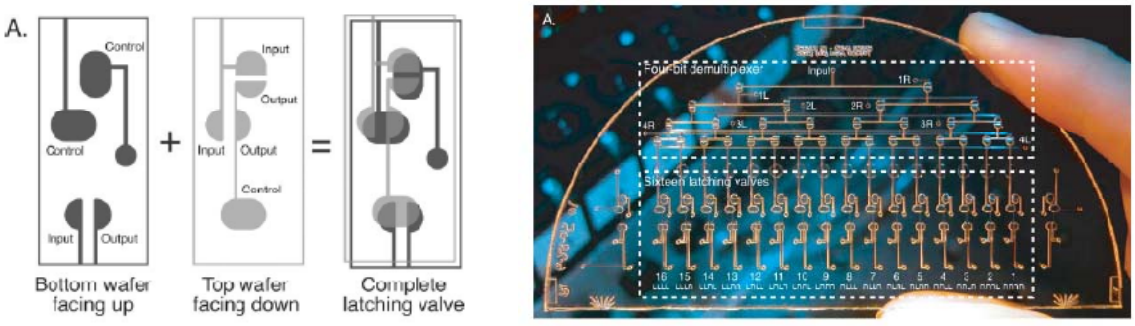


**Figure 68:** Single Latching Valve (Left), Sixteen Multiplexed Latching Valves (Right) [35]

The existing technologies have shown the response time of logical structures is lower than the frequency of 50 Hz we desired. Based on the researches we have studied, a more feasible approach for achieving 50 Hz frequency would be to induce oscillations in the system by using mechanism like solenoid that has high frequency outputs.

**Conclusion:** There is certainly a tradeoff between the simplification of the system using fluidic logic and the device behavior characteristic that we specified. Based on the results gathered by various research groups, we would like to keep fluidic logic as an option for future optimization of our device and to have a tactile display that meets our specifications for now.

## APPENDIX G

### Material Selection Assignment (Functional Performance)

Our project only requires for the tactile array to be fabricated while the rest of the components are ordered from external sources. The array consists of top and bottom bases with thin membrane on top. They are made from the same material and will be bonded together as one component.

The array will have 16 channels where a tank with regulator and valves will supply CO2 gas with a pressure of 30 Psi at frequencies up to 200 Hz. The material has to be strong enough to withstand this pressure and has the flexibility to form the "bubbles" to stimulate the users' skin. Due to low forces (< 1N) applied to the membrane, we are less concerned with failure and more focused on the elasticity of the membrane.

It is also important that the material can be molded accurately up to 0.25 mm for us to create the bubbles and channels. Durability is also important because the array will interact extensively with human skin and be exposed to various compounds and substances.

Our objective is to find a material with minimum stiffness (Young's Modulus) and density while having a high resistance to water, acids, alkalis, and sunlight (UV radiation). From the last four materials, we choose PDMS as it is the widely available and commonly used in biological application; have relatively low Young's modulus, lowest density and able to be accurately molded. We also have access to local fluid laboratory where experts have been using the PDMS for their research and can assist us in the process of fabrication.

### Material Selection Assignment (Environmental Performance)

As explained in the material selection section, several materials that we have considered are PDMS and other silicones. However, due to the limited selection in the Simapro 7.1, we will use other thermoplastic elastomers, Polybutadine (PBD) and Styrene Butadiene Rubber (SBR) and compare them on their impact to the environment. The entire fabricated part's dimensions are 50 x 50x 5.15 mm as seen in Appendix A and its approximate weight is 15g. Taking into account the amount of materials used during the manufacturing process, we will compare 100g of PBD and SBR.

From the Figure 71 to 74, we can see that PBD appears to have a higher overall environmental impact. Considering similar life cycle of both materials, the PBD will cause greater life cycle environmental impact than SBR. PBD has higher impact in the respiratory inorganic and climate change, although SBR is more dangerous due to the presence of carcinogens, greater amount of land use, minerals, and cause more ecotoxicity and acidification/eutrophication. From this material selection, we will choose PBD due to the absence of carcinogen produced and overall less dangerous impact to the environment.

This analysis is based on the closest to the actual material, Polydimethylsiloxane (PDMS). Given more resources, we would like to analyze and compare the impact of PDMS and other Silicone polymers to the environment. However, due to the relatively small amount of material used and its impact to the environment, we are more concerned with a material's functional performance during our material selection.

**Manufacturing Process Selection**

Our product is an electronically-controlled pneumatic tactile display that stimulates the skin's mechanoreceptors by using inflatable bubbles. This product will be useful as a laboratory instrument that can help the experts in the field of tactile perception of the skin. There are many researchers in the world that created their own models or products to test human tactile perception, most of them with varying results. Our product can be used as a standardized equipment to be used in these tests as our design emphasizes on the flexibility of the desired force, frequency, displacement and spacing of the actuators that can be varied according to the users' needs.

Although we can see 100 units of our product being used by professors all around the world, our production volume will be close to 1 or 10 due to the specifications our users might want. Our tactile pad can be made to stimulate different type of mechanoreceptors in the skin by varying its tactors size, spacing and size of the pad itself.

The specification constraint for our product will be the size of the plasma oven as we could not justify the cost of buying a larger one; which can easily reach $10,000. The cost for using the plasma oven is unknown as it works just like a common oven so we are unable to find the cost of operating one. The maximum size of display that can be produced with the current oven is 1ft x 1 ft (305 mm x 305 mm). The other factor is the membrane thickness as it gets difficult to remove under 0.1 mm. We create an aluminum mold for our display but we can use other metal to reduce the cost depending on the size of the display. Although it is not a significant cost reduction as a 1ft x 1ft x 1.02mm sheet is only $5.40 and we can make about six molds. A smaller display will be more expensive to fabricate as we need to use a silicon-wafer method while larger display can be molded using a milled metal. Larger displays also have larger production volume as we can make a larger mold that can make 5 to 10 units at one time.

One significant difference that can be made during the mass manufacturing of our products is the fabrication of a better mold that will allow us to skip the threading process of the display which raises significant accuracy issue.

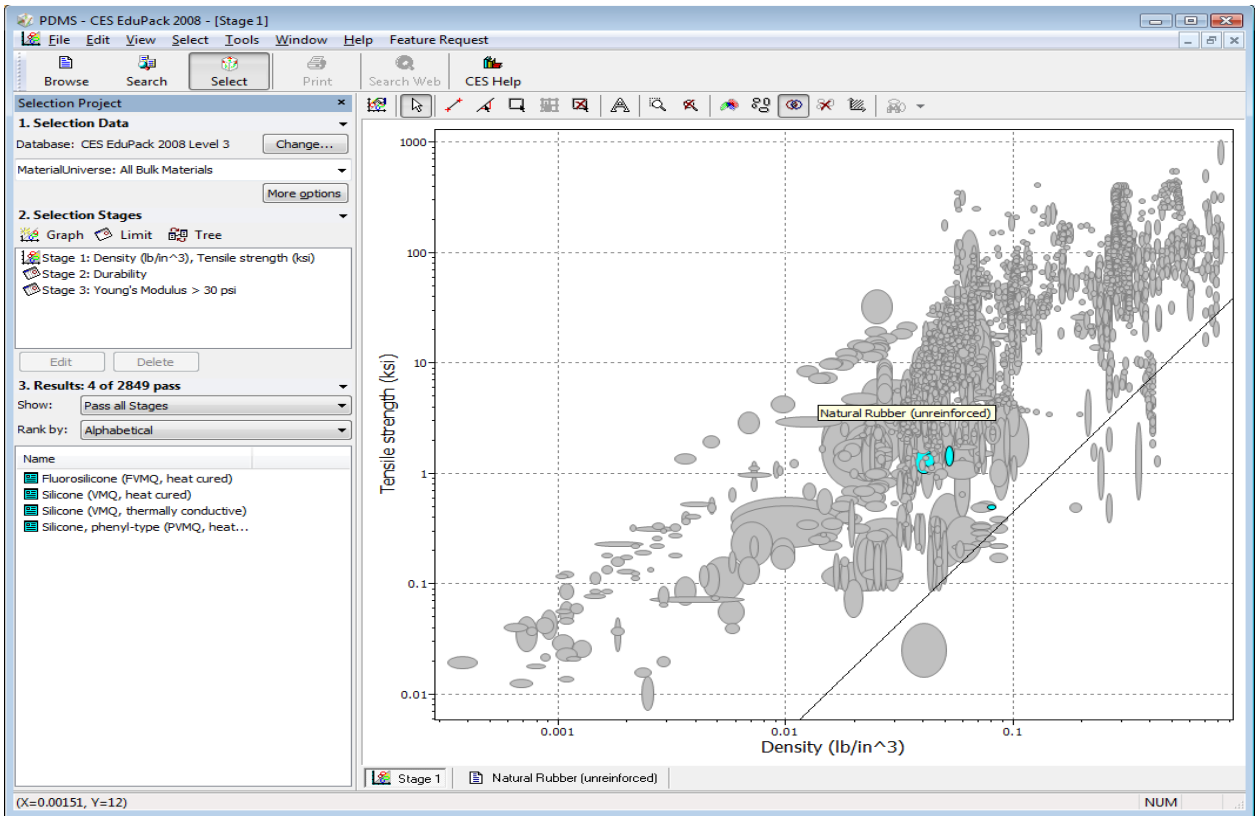


**Figure 69: Material Selections Compared to Natural Rubber**

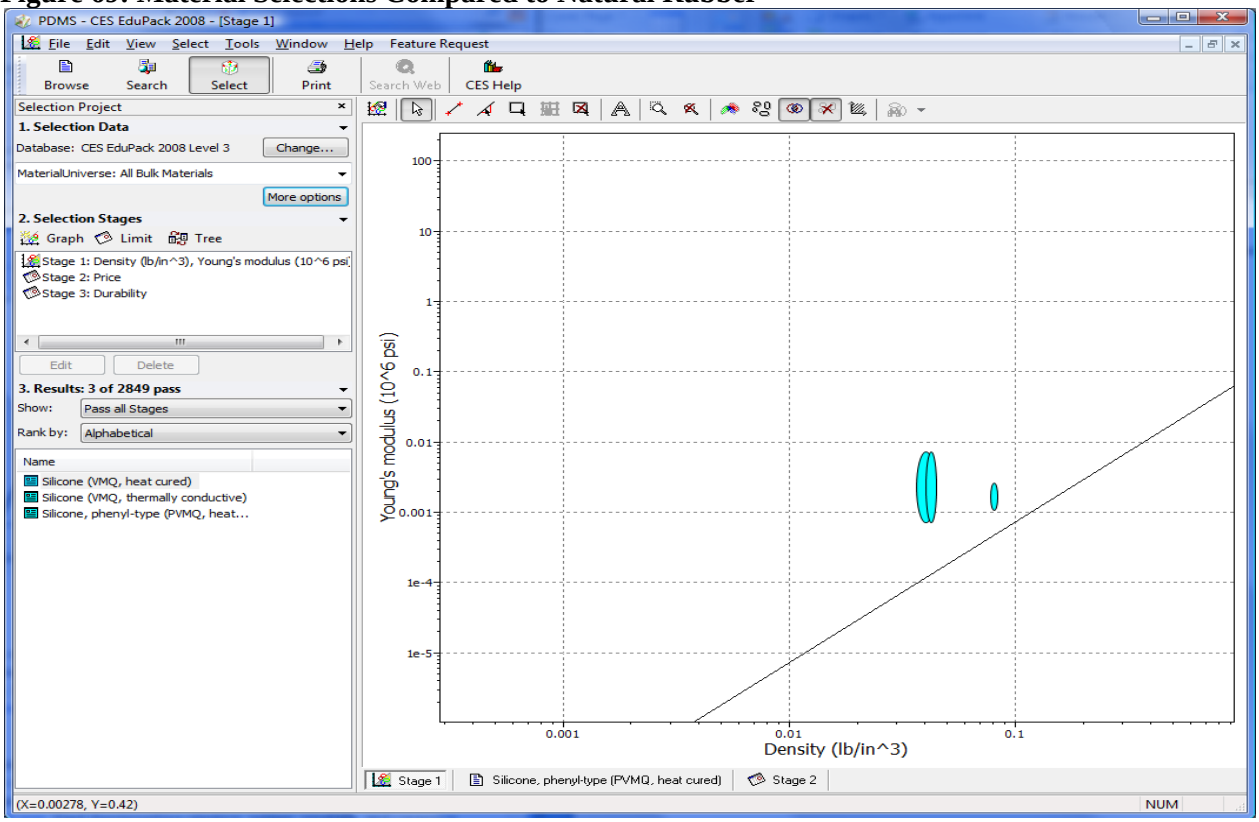


**Figure 70: Final Three Materials in the CES 2008**

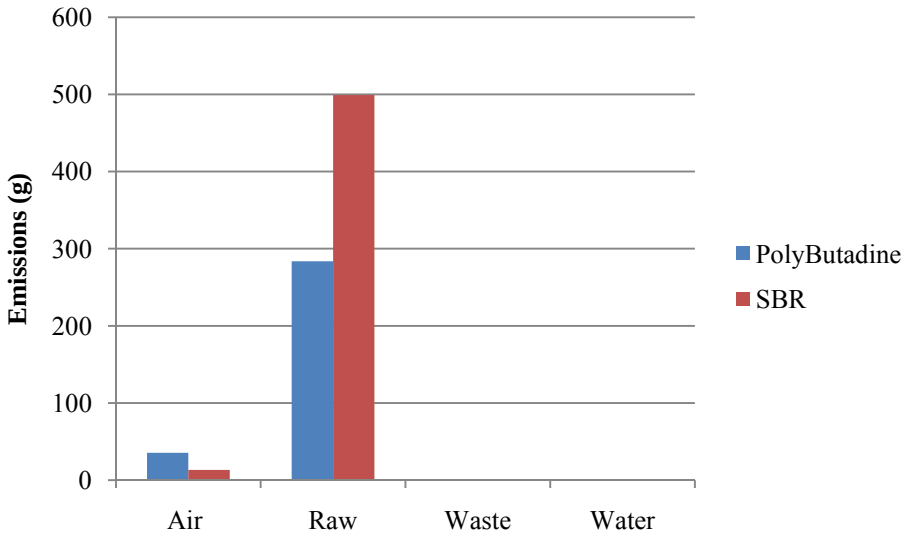


**Figure 71: Total Emissions of Polybutadine and SBR**

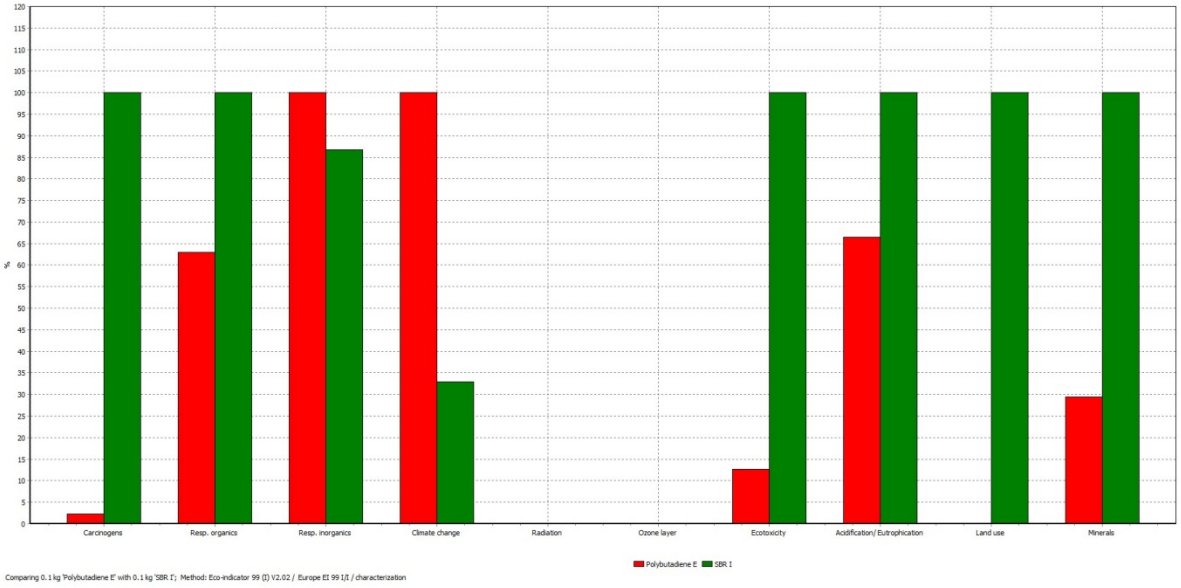


**Figure 72: Relative Impacts in Disaggregated Damage Categories**

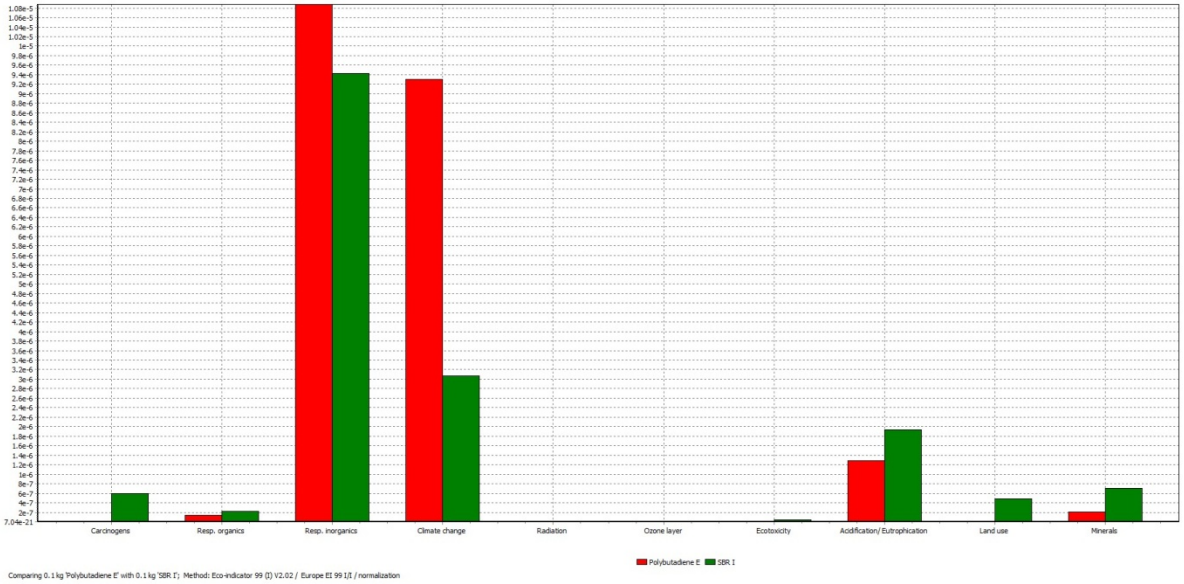


**Figure 73: Normalized Score in Human Health, Eco-Toxicity, and Resource Categories**

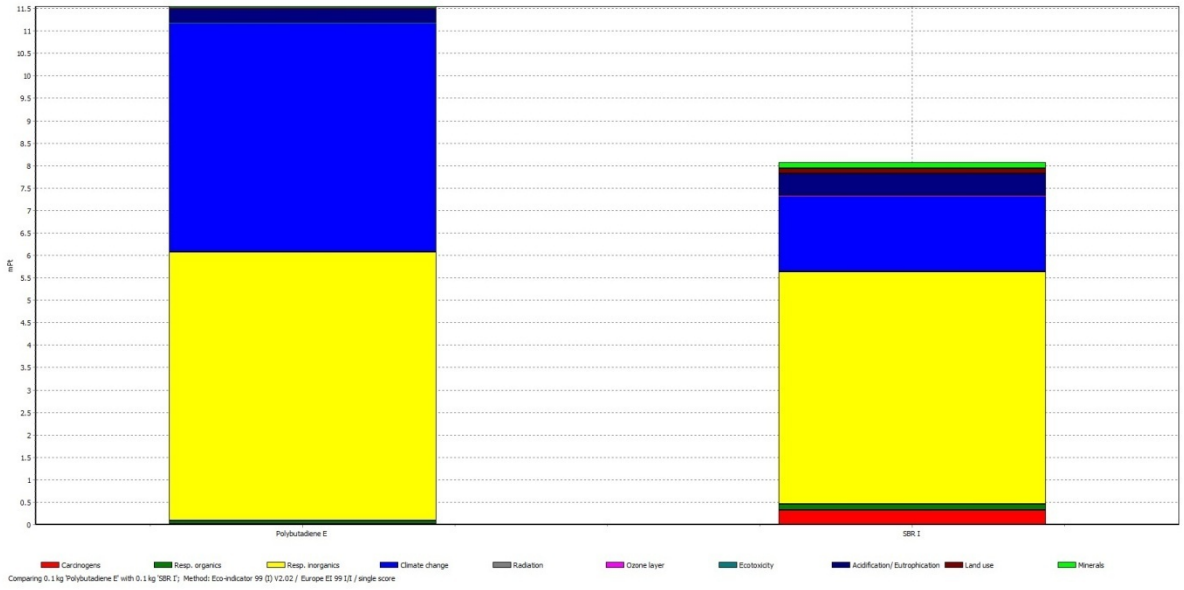


**Figure 74: Single Score Comparison in "Points"**

**REFERENCES**


1. Dong, K., & Srinivasan, S. K. (2005). *Perceptual and biomechanical frequency response of human skin: implication for design of tactile displays.*

2. Biggs, J., Srinivasan, M.A., (2002) "Tangential versus Normal Displacements of Skin: Relative Effectiveness for Producing Tactile Sensations", Laboratory for Human and Machine Haptics, Massachusetts Institute of Technology, USA

3. Velazquez R., Pissaloux, E. E., (2008) "Tactile Displays in Human-Machine Interaction: Four Case Studies", The International Journal of Virtual Reality, pp.51-68

4. Jones, L. A., Lederman, S. J. (2006). *Human Hand Function.* Oxford University Press

5. Bolanowski Jr, S., Gescheider, G., Verrillo, R., & Checkosky, C. (1988). Four channels mediate the mechanical aspects of touch. The Journal of the Acoustical Society of America, 84, 1680.

6. King, C. H., Culjat, M. O., Franco, M. L., Bisley, J. W., Dutson, E., & Grundfest, W. S. (2008). Optimization of a Pneumatic Balloon Tactile Display for Robot-Assisted Surgery Based on Human Perception. *IEEE Transactions on Biomedical Engineering*, 55(11), 2593-2600.

7. Kim, Y., Oakley, I., & Ryu, J. (2006). Design and psychophysical evaluation of pneumatic tactile display. *2006 SICE-ICASE International Joint Conference*, (pp. 4845-4850).

8. Fearing, R.S., Moy, G., Wagner, C.(2000). A Compliant Tactile Display for Teletaction. Robotics and Automation, 2000. Proceedings. ICRA '00. IEEE International Conference **.**

9. Wu, X., Yuan, G., & Yoon, Y.K. (2008). Kinematically-stabilized microbubble actuator arrays. *Journal of Microelectromechanical Systems* 17(1), 124-132.

10. Thompson et al., "Resist Processing," *in Introduction to Microlithography*, 2nd ed. Washington, DC: American Chemical Society, pp. 305-313 (1994)

11. Aluru, N., Armani, D., Liu, C. (1999) Re-configurable fluid circuits by PDMS elastomer micromachining. MEMS '99. Twelfth IEEE International Conference, 222-227

12. Timoshenko, S., and Woinosky-Krieger, S. (1987).*Theory of Plates and Shells.* New York : McGraw–Hill.

13. Cronis, N., Jeong, K., Lee, P.L., Liu, G.(2004). Tunable microdoublet lens array. Optical Society of America, 12, 2494-2500.

14. Mcdonald, J.C., Whitesides, G.M.(2001). Poly(dimethylsiloxane) as a Material for Fabricating Microfluidic Devices. Accounts of Chemical Research, 35, 491-499

15. Pawluk, D. T. V., & Howe, R. D. (1999). Dynamic lumped element response of the human fingerpad. Transactions-American Society Of Mechanical Engineers Journal Of Biomechanical Engineering, 121, 178-183.

16. Wu, J. Z., Dong, R. G., & Welcome, D. E. (2006). *Analysis of the point mechanical impedance of fingerpad in vibration.* Medical Engineering and Physics, 28(8), 816-826.

17. Granta Design Limited: Cambridge Engineering Selector Edupack 2008 (Version 4.8.0) [Software]. University of Michigan.

18. Busch, J. D. & Gilbertson, R. G. (1996). A survey of micro-actuator technologies for future spacecraft missions. The Journal of the British Interplanetary Society, 49, 129-138.

19. Iwamoto, T., Maeda, T., & Shinoda, H. (2001). Focused Ultrasound for Tactile Feeling Display. In *The Eleventh International Conference on Artificial Reality and Telexistence (ICAT 2001*).

20. Iwamoto, T., Akaho, D., & Shinoda, H. (2004). High Resolution Tactile Display Using Acoustic Radiation Pressure. *SICE 2004 Annual Conference* (pp. 1239-1244). Japan: Hokkaido Institute of Technology.

21. Shikida, M., Imamura, T., Ukai, S., Miyaji, T., & Sato, K. (2008). Fabrication of a bubble-driven arrayed actuator for a tactile display. *Journal of Micromechanics and Microengineering*, 6, 065012 (9 pp.).

22. Davidson, R., Liu, Y., & Taylor, P. (2005). Touch sensitive electrorheological fluid based tactile display. Smart Materials And Structures, 14, 1563-1568.

23. Davidson, R.I., Liu, Y., Ngu, J.D., Taylor, P.M., Zarraga, J.M.C.(2004). Single cell magnetorheological fluid based tactile display. Elsevier, Displays 26, 29-35.

24. Choi, H. R., Jung, K., Koo, I. M., Koo, J. C., Lee, Y. K., & Nam, J. (2008). Development of Soft-Actuator-Based Wearable Tactile Display. IEEE Transactions of Robotics, 24 (3), 549-558.

25. Citerin, J. & Kheddar, A. (2006). An MRI-compatible tactile display device based on IPN-CP pastille-shaped actuators. Structures and Materials, 6168, 61681C1-61681C12.

26. Hayward, V., & Cruz-Hernandez, M. (2000). *Tactile display device using distributed lateral skin stretch*.Henderson, D. A. Novel Piezo Motor Enables Positive Displacement Microfluidic Pump. *Stroke (mm), 50*, 10.

27. Pasquero, J., & Hayward, V. (2003). *STReSS: A Practical Tactile Display System with One Millimeter Spatial Resolution and 700 Hz Refresh Rate*.

28. Kim, S.-C. (2008). SaLT: Small and lightweight tactile display using ultrasonic actuators. *Proceedings of the 17th IEEE International Symposium on Robot and Human Interactive Communication, RO-MAN*, 430-435.

29. Streque, J. (2008). *Electromagnetic actuation based on MEMS technology for tactile display*. Lecture Notes in Computer Science (including subseries Lecture Notes in Artificial Intelligence and Lecture Notes in Bioinformatics), 5024 LNCS, 437-446.

30. Velazquez, R. (2006). A compact tactile display for the blind with shape memory alloys. *Proceedings - IEEE International Conference on Robotics and Automation, 2006*, 3905-3910.

31. Jungmann, M., & Schlaak, H. F. (2002). *Miniaturised Electrostatic Tactile Display with High Structural Compliance*.

32. Goethals, P., Lintermans, H., Sette, M., Reynaerts, D., & Van Brussel, H. (2008). *Powerful Compact Tactile Display with Microhydraulic Actuators*. Lecture Note on Computer Science, 5024, 447.

33. Hallinan, K. P., Kang, S., Kashani, R. (2000). Micro-Scale Electohydrodynamic Pumped High Performance Actuation. Journal of Intelligent Material Systems and Structures, 11, 343-350.

34. Chang, H., Huang, M., Lai, C., Tsou, C.(2007). Pneumatic-Controlled Fluidic Microdevices for Executing NOT, NOR, and NAND Logic Functions. Japanese Journal of Applied Physics, 47, 1780-1786.

35. Grover, W.H. , Ivester, R.H.C., Jensen, E.C. (2006). Development and multiplexed control of latching pneumatic values using microfluidic logical structures. Royal Society of Chemistry, 6, 623-631.